2016

Characterization Of 1-Deoxy-D-Xylulose 5-Phosphate Reductoisomerase (Dxr) From Vibrio Vulnificus

Nikita K. Ussin
University of South Carolina

Characterization Of 1-Deoxy-D-Xylulose 5-Phosphate Reductoisomerase (Dxr) From *Vibrio Vulnificus*

by

Nikita K. Ussin

Bachelor of Science
Xavier University of Louisiana; 2007

Master of Science in Public Health
Tulane University; 2010

Submitted in Partial Fulfillment of the Requirements

For the Degree of Master of Science in

Chemistry

College of Arts and Sciences

University of South Carolina

2016

Accepted by:

Maksymilian Chruszcz, Director of Thesis

Caryn Outten, Reader

Paul Allen Miller, Vice Provost and Interim Dean of Graduate Studies

Abstract

Vibrio vulnificus, a gram-negative bacterium, is the leading cause of seafood-borne illnesses and mortality in the United States. Previous studies of bacterial pathogens have identified a metabolite essential to *V. vulnificus* growth and function. 1-deoxy-D-xylulose 5-phosphate reductoisomerase (Dxr) is an essential enzyme in the viability of many bacteria and catalyzes the rearrangement of 1-deoxy-D-xylulose 5-phosphate (Dxp) to 2-C-methylerythritol 4-phosphate (MEP) within the MEP pathway found in plants and bacteria. Previous studies have been conducted to characterize Dxr homologs from other pathogens including *E. coli, M. tuberculosis,* and *P. falciparum.* Information on the structural and enzymatic characteristics of Dxr from *Vibrio vulnificus*, or VvDxr, is not known. In this study, we show for the first time apo and ligand-bound structures of VvDxr. The structures are from both His-tag cleaved (cut) and uncleaved (uncut) protein. Using Dxr homologs, we identify similarities in the structural characteristics among these enzymes. The binding characteristics were also studied to identify parallels between the enzyme's affinity for metals and inhibitors. Our findings will provide basis for design of Dxr inhibitors that may find application as antimicrobial compounds.

Table of Contents

List of Tables

List of Figures

List of Abbreviations

2,6 PDC ..... 2,6 Pyridinedicarboxylic acid

ANL ..... Argonne National Laboratory

APS ..... Advanced Photon Source

DMAPP ..... Dimethylallyl pyrophosphate

Dxs ..... 1-deoxyD-xylulose synthase

Dxp 1-deoxy-D-xylulose 5-phosphate

Dxr ..... 1-deoxy-D-xylulose 5-phosphate reductoisomerase

DSF ..... Differential Scanning Fluorimetry

EcDxr ..... Dxr from *Escherichia coli*

IPP ..... Isopentenyl diphosphate

ITC ..... Isothermal Titration Calorimetry

MEP 2-C-methylerythritol 4-phosphate

MtDxr ..... Dxr from *Mycobacterium tuberculosis*

NADPH ..... Nicotinamide adenine dinucleotide reduced phosphate

PDB ..... Protein Data Bank

PfDxr ..... Dxr from *Plasmodium falciparum*

SER-CAT ..... Southeastern Regional Collaborative Access Team

VvDxr ..... Dxr from *Vibrio vulnificus*

Chapter 1

Introduction

Vibrio vulnificus is a gram- negative bacterium viable in warm, brackish, coastal water. This particular species of *Vibrio* gains access to the body by ingestion of contaminated raw seafood or through absorption into an open wound that has been in *vulnificus* contaminated water [1-3]. Immunocompromised individuals are more susceptible to *V. vulnificus* infections, and the resulting symptoms are more severe in comparison to healthy individuals [3-4]. *V. vulnificus* is the leading cause of seafood-borne mortality in the United States with fatalities of over sixty percent due to primary septicemia and over twenty percent resulting from open wound contamination [1-5]. To avoid severe infection and fatality, immediate diagnosis and treatment is urged.

Previous studies have identified an enzymatic pathway, ubiquitous in most bacteria and bacteria (Fig 1.1) [6-7]. The non-mevalonate or MEP pathway produces the isoprenoids, isopentenyl diphosphate (IPP) and dimethylallyl pyrophosphate (DMAPP). These compounds are essential precursors to the biosynthesis of steroids necessary for vital functions within the bacterial cell, including metabolism functions and cell wall generation [8]. Because this pathway is absent in mammals, it is an ideal target for drug studies. Dxr catalyzes the reduction and isomerization of 1-deoxy-D-xylulose 5-phosphate (Dxp) to 2-C-methylerythritol 4-phosphate (MEP). This reaction is the committed step in the pathway, and NADPH

and divalent cation are cofactors. A study seeking to identify essential metabolites in this species of Vibrio indicated that knocking down the gene encoding for Dxr rendered the bacteria nonviable [6]. A vast amount of other infections is caused by pathogenic bacteria that also utilize the MEP pathway, including pneumonia, cholera, and gonorrhea [8]. Inhibition of the critical Dxr enzyme can lead to eradication of *Vibrio vulnificus* and a host of other pathogens.

Presently, fosmidomycin and FR-900098, current antimalarial agents, have been very effective in inhibiting the activity of Dxr. Previous studies have also identified a different class of antibiotics, bisphosphonates, which are also capable of inhibiting the activity of this enzyme [9-11]. Another Dxr inhibitor that has gained interest is 2,6 Pyridinedicarboxylic acid (2,6 PDC) derivative [12]. As *Vibrio vulnificus* infections have increased in the past few years, details on the VvDxr enzyme and how it interacts with this compound can provide insight into the development of a new class of PDC-based inhibitors.

The structure of Dxr has been determined via crystallography and studied in organisms including *Escherichia coli* (EcDxr), *Mycobacterium tuberculosis* (MtDxr), and *Plasmodium falciparum* (PfDxr). The enzyme crystallizes as a homodimer, and each subunit consists of two domains: a catalytic domain and a C-terminal domain [13-15]. The residues making up the active site are highly conserved. Although the structures of other Dxr homologs have been determined, there has been no structure determined for the VvDxr enzyme until now.

We are interested in the isolation and structural determination of VvDxr. We show both the apo and ligand-bound protein structures of VvDxrprotein, either with

the polyhistidine tag uncleaved (uncut) or cleaved (cut). Details of the polyhistidine tag and its removal can be found in the Material and Methods section. We alsos provide information of their similarities to the previously studied homologs. In this study, we show that VvDxr shares similar structural characteristics to other homologs. Additionally, we show that metal cofactors promote thermal stability of the VvDxr protein.

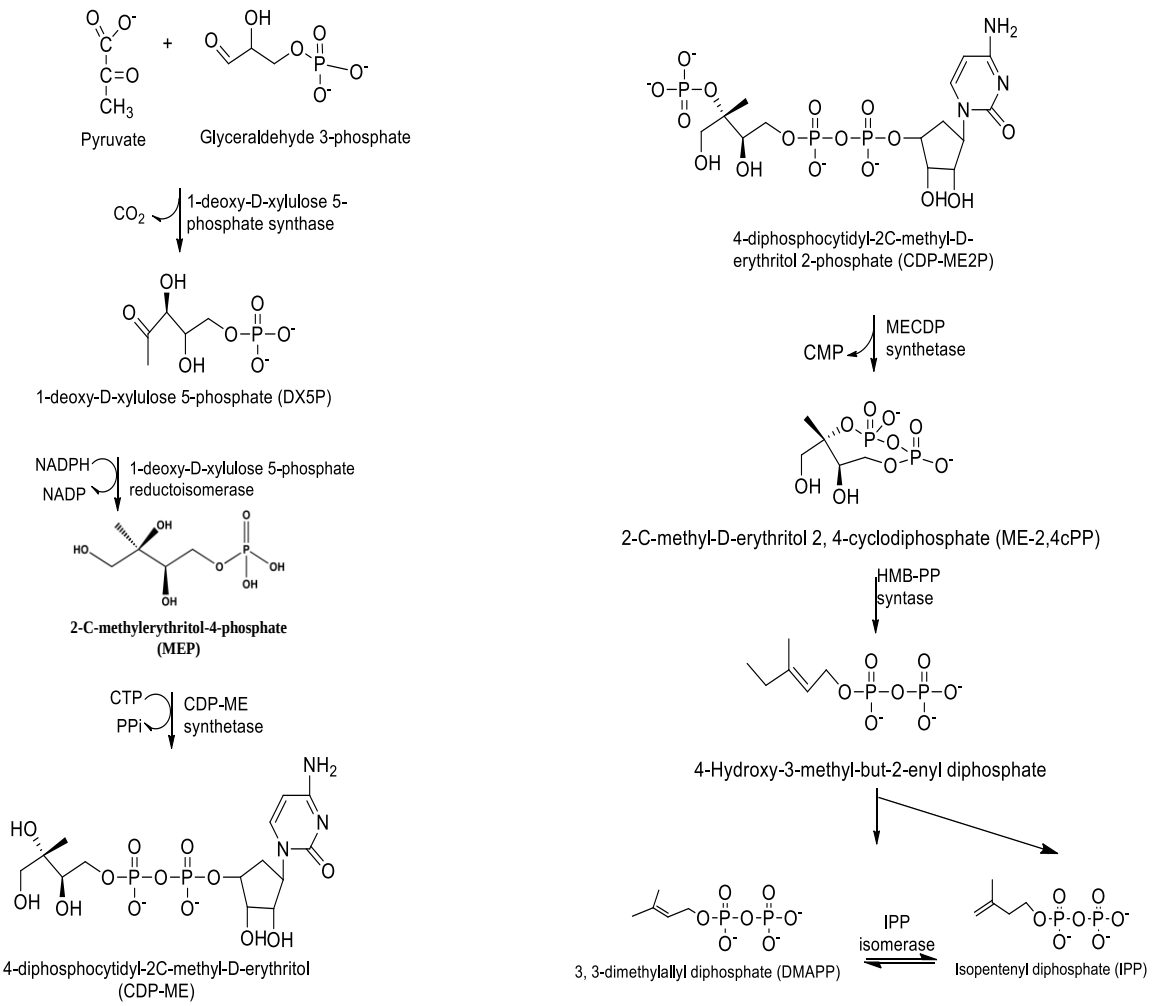

Figure 1.1. Non-mevalonate or MEP pathway. This pathway is found in most plants and bacteria and is named for 2-C-methyl-D-erythrito 4-phosphate (MEP) [7]

Chapter 2
Results and Discussion

Overexpression and purification of VvDxr

VvDxr was overexpressed with the initial isolation yielding approximately 150 mg of the protein per 1 L of culture. Protein purity was confirmed using SDS-Page gel (Fig 2.1) and mass spectrometry (Fig 2.2). The protein was further purified by gel filtration. The resulting elution profile contained one sharp peak corresponding to the molecular weightof a VvDxr dimer (~88 kDa). Cleavage of the protein's polyhistidine tag was successful, and the cut VvDxr was verified after SDS-Page gel identification prior to additional purification by gel filtration. (Fig 2.3). These results indicate that VvDxr is a dimer in solution.

VvDxr Crystallization

All crystallization experiments were conducted at 293 K. VvDxr crystals were identified within 48 hours using protein from the initial purification of VvDxr. Crystals were identified in a variety of conditions including Wizard Classic 1 (Rigaku, Bainbridge Island, WA) conditions 9, 28, 34, 41, and 47, and Wizard Classic 2 (Rigaku, Bainbridge Island, WA) conditions 10, 29, 33, 37, 46, and 48 (Table 1).

The aforementioned conditions were remade in our lab, and crystallization drops were set using the hanging drop vapor diffusion method. Crystals identified from the optimized screens were Wizard Classic 2 conditions 33 and

37. These screens were further optimized by small increments to produce the conditions found in Tables 2 and 3. From the optimized conditions, crystals were formed, and we were later able to determine the first structure of VvDxr (Fig. 2.4).

2.1 VvDxr Sequence Analysis

VvDxr contains 402 residues in each chain of the homodimeric structure. The sequence of VvDxr was aligned with previously determined Dxr homologs. The percent identity is listed in the legend of Figure 2.5. Sequence conservation was mapped on to VvDxr structure using EcDxr and ligands present in the active site in order to compare the active site of this protein with homologs. Figure 2.6 shows sequence conservation mapped on VvDxr structure [22-23]. The analysis of the sequence conservation reveals that the highly conserved residues cluster near of both the active site and flexible loop.

2.2 Structural Analysis

The first diffraction data were obtained from a VvDxr crystal grown from an optimized condtion: 0.1 M Sodium citrate pH 5.0, 1.2 M Ammonium phosphate and 0.2 M NaCl. The native crystal was formed from uncut protein. The crystal formed had $C222_1$ symmetry and a dimeric assembly in the asymmetric unit. Further analysis of the crystal structure revealed a clearly distinguishable N-terminal and C-terminal domain, along with a highly conserved binding domain or active site.

Subsequent diffraction data were obtained from crystals grown in the following conditions: (1) 0.1 M Sodium citrate pH 5.0, 0.8 M Ammonium phosphate, 0.2 M Sodium chloride and (2) 0.1 M Sodium citrate pH 5.5, 0.8 M Ammonium phosphate, 0.2 M Sodium chloride. Crystals formed in conditions (1) and (2) were

allowed to form before soaking the crystals in conditions that only differed in the progressively decreasing phosphate Ammonium phosphate concentrations (0.8 M, 0.6 M, 0.4 M, 0.2 M, 0 M Ammonium phosphate). Solid manganese (II) chloride and 2 mM fosmidomycin (condition 1) and 2 mM FR900098 (condition 2) were added to the cryo-protectant drop.

Further crystallization experiments continued utilizing Index screen (Hampton Resarch, Aiso Viejo Dimensions/Rigaku CA) and the sitting drop vapor diffusion method. Despite the success of the hanging drop experiments, crystals were formed, but not in the same time frame as before. The crystals produced in 1.0 M Succinic acid pH 7.0, 0.1 M HEPES pH 7.0, 1% w/v PEG 2000 were free of phosphate and sulfate and diffracted. These conditions were further optimized, and drops were set using the sitting drop vapor diffusion method. Despite the various conditions, all crystal structures had $C222_1$ symmetry and a dimeric assembly in the asymmetric unit. Tables 2.4 and 2.5 outline the data collection and processing details for all deposited structures. Tables 2.6 and 2.7 detail the refinement statistics for these structures.

2.3 VvDxr Overall analysis

The first structure to be determined was native uncut VvDxr. All VvDxr structures determined thereafter used this structure as a model. The VvDxr apo-structure was determined at 2.35 Å resolution. VvDxr crystallized as a homodimer with each monomer containing a phosphate ion in the same position in active site, and the flexible loops in both monomers are ordered. This model of VvDxr was

deposited to the PDB with accession code 5KQO. Two structures were determined after working to 'soak out' the phosphate and co-crystallize with fosmidomycin or FR900098. In both structures, the VvDxr protein crystallized as a homodimer. Although the protein did not crystallize with neither fosmidomycin nor FR900098, manganese ions in are present in both active sites instead of phosphate. VvDxr in the presence of FR900098 has an ordered flexible loop for chain B, but not for chain A. We assume this to be due to the negative cooperativity of the Dxr enzyme [16]. These His-tag cleaved structures were deposited to the PDB with accession codes, 5SK1 and 5KRR, respectively, and determined at 2.4 Å and 2.5 Å resolutions.

After successfully crystallizing VvDxr in the absence of phosphate and sulfate, we were able to determine a structure of cut VvDxr protein. The protein was crystallized in the absence of ligands. The electron density around the flexible loop in chain A is disordered. Molecular replacement was performed using 5KQO as a model. The structure was determined at 2.2 Å and deposited to the PDB with accession code 5KRY.

2.4 Active Site

The first structure of VvDxr contained a phosphate in the active site. The structure of Dxr contained a phosphate ion in the active site. Superposition of VvDxr with PfDxr in complex with FR900098 (PDB code: 3AUA) showed the phosphate ions to be located in the active site. Figure 2. 7 shows that the ions are located in the same position in the homologs. The residues making up the highly conserved active site were: G11, S12, I13, G14, K37, N38, A123, L122, A123,

N124, K125, E126, D150, S151, E152 and H153. There is also a highly conserved flexible loop made up by residues H209, P210, N211, W212 (Fig 2.8).

After multiple structures have been determined with phosphate in the active site, we continued to soak the protein in either NADPH, FR900098 or fosmidomycin in anticipation that the inhibitors will co-crystallize with the protein. This discovery led us to focus on crystallizing VvDxr in the previously mentioned condition and then remove the phosphate and sulfate by soaking them out of the crystal. Another method we tried was to crystallize VvDxr in conditions containing no phosphate or sulfate. We were able to determine two structures after using this soaking out technique. However, the inhibitors did not crystallize with the protein. Instead, the divalent cation was crystallized in the active site.

2.5 VvDxr in Complex with Metals

Previous structures of Dxr homologs deposited in the PDB are in complex with either NADPH, a divalent cation, a previously studied Dxr inhibitor or a combination of these [10][15-16]. Our study sought to determine the crystal structure of VvDxr in complex with cofactors and/or metals. Although efforts to co-crystallize the protein with inhibitors and/or NADPH cofactor was unsuccessful, we were able to determine the structures of multiple VvDxr structures in complex with metal cations.

Crystals were also grown in the presence of 0.8 M Succinic acid. Diffraction data was collected and a structure was determined. In the active site, there was a magnesium ion in the active site. To quantify the amount of magnesium present

in the active site, our sample was tested using Inductively Coupled Plasma-Mass Spectrometry. This form of mass spectrometry is used to detect and analyze the metals present in a sample. The results of the experiment performed by Dr. Lijian He (Mass Spectrometry Manager, University of South Carolina) suggested there is approximately 0.5 mole of magnesium ion per chain in our VvDxr structure. These results correspond to the density present in the active sites of our structure.

Differential Scanning Fluorimetry

VvDxr stability was measured using Differential Scanning Fluorimetry (DSF). Soluble VvDxr protein is incubated with Sypro-orange, a fluorescent probe. As the protein is heated, the hydrophobic residues are exposed, and the probe binds to the exposed residues. The temperature at which the protein fluoresces denotes the melting temperature and thermal stability of the protein [22]. In our experiment, we wanted to determine the thermal stability of native VvDxr and then measure which ligands may promote an increase in thermal stability. By identifying an increase in the melting temperature of VvDxr in the presence of ligand, we assumed the ligand binds to our protein.

The cut VvDxr is slightly more stable than uncut VvDxr (Fig 2.9). VvDxr remained more stable in the presence of divalent cations, in particular manganese (II) chloride, magnesium (II) chloride, and calcium (II) chloride (Fig 2.10). The thermal stability of the protein was also tested in the presence of NADPH and manganese (II) chloride (Fig 2.11). The VvDxr melting temperature increased, confirming our hypothesis that VvDxr is more stable in the presence of NADPH and magnesium.

To identify other ligands that may promote thermal stability of the VvDxr protein, the experiment was carried out in the presence of 386 different ligands. Initially, our aim was to also study the thermal stability of VvDxr with its' substrate, 1-deoxy-D-xylulose 5 phosphate, or Dxp. However, Dxp is too costly to purchase or synthesize. Figures 2.12-14 provides the results. Divalent cations were among the compounds to promote thermal stability. After identifying compounds promoting thermal stability, crystallization experiments were carried using various phosphate free screens and all of the ligands from the DSF screen and the sitting drop vapor diffusion method. Our purpose was to co-crystallize VvDxr in complex with the ligands shown to increase the protein's melting temperature and identify inhibitors or homologues Dxp. Contrary to our results, we were able to determine a structure of VvDxr in complex with arginine, a compound that did not improve thermal stability. The crystal was grown in 0.8 M Sodium potassium tartrate, 20% PEG 3350, 5 mM Arginine, solved at 2.3 Å and deposited to the PDB with the accession code of 5KRV. Interestingly, the arginine is not found anywhere near the active site (Fig. 2.15).

Isothermal Titration Calorimetry

After identifying metals that co-crystallize or promote thermal stability of VvDxr, Isothermal Titration Calorimetry (ITC) was performed to study the binding thermodynamics. From the results, we are able to calculate: number of active sites (N), dissociation constant (K), change in enthalpy (ΔH), change in entropy (ΔS), and Gibbs free energy (ΔG) values. The results are consistent with ITC studies

from Dxr homologs [16-17]. VvDxr was first tested with either manganese (II) chloride or magnesium (II) chloride in the buffer solution. NADPH was injected into the protein solution, and the resulting isotherm is show in Figure 2.16. The results affirm our hypothesis: the binding of VvDxr to NADPH is exothermic. The thermodynamic parameters observed are similar to those of other Dxr homologs. NADH binding was also tested to prove that NADH does not bind to VvDxr. The results indicated that no binding occurred.

ITC was also used to determine if there was any indication of binding of ligands or potential inhibitors binding to VvDxr. The compounds shown to promote VvDxr thermal stability were first run with buffer only to ensure there was no ligand-ligand binding. Afterwards, ligands were run with protein. Using 2,6 Pyridinedicarboxylic acid as the ligand, the thermodynamics of binding was measured (Fig. 2.17). There is indication of the ligand-protein binding. Further studies are necessary to determine if 2,6 PDC binds in the active site of the protein.

Conclusion and Future Directions

The crystal structures of VvDxr were all solved in the same space group, and without ligands bound in the active site. This happens in the presence or absence of phosphate, sulfate, or metals. It is possible that the protein prefers a certain crystallization form and thereby prevents the binding of ligands. Co-crystallization studies should continue to incorporate the cofactor(s) and/or inhibitors in the active site. Current enzymatic studies of 1-deoxy-D-xylulose-5-phosphate synthase (Dxs) to produce DXP for enzymatic assays involving Dxr have been inconclusive, but further analysis can provide more insight into the

characteristics of this protein. . Although there is indication of 2,6 PDC binding to our protein, additional studies with this and other ligands may lead to the design of a new class of inhibitors.

TABLE 2.1. Wizard crystallization conditions.

Crystallization conditions for VvDxr crystals identified after initial screening

Screen	Condition #	Condition contents
Wizard Classic 1	9	1000 mM Ammonium phosphate dibasic, 100 mM Sodium acetate/Acetic acid pH 4.5
	28	20% (w/v) PEG
	34	10 % (w/v) PEG 8000, 100 mM Imidazole/Hydrochloric acid pH 8.0
	41	2000 mM Ammonium sulfate, 100 mM Tris base/hydrochloric acid pH 7.0, 200 mM Lithium sulfate
	47	2500 mM Sodium chloride, 100 mM imidazole/Hydrochloric acid pH 8.0, 200 mM Zinc acetate
Wizard Classic 2	10	1000 mM Ammonium phosphate dibasic, 100 mM Tris base/Hydrochloric acid pH 8.5
	29	1260 mM Ammonium sulfate, 100 mM CHES/Sodium hydroxide pH 9.5, 00 mM Sodium chloride
	33	1000 mM Ammonium phosphate dibasic, 100 mM Sodium citrate tribasic/Citric acid pH 5.5, 200 mM Sodium chloride
	37	1000 mM Potassium sodium tartrate, 100 mM Tris base/Hydrochloric acid pH 7.0, 200 mM Lithium sulfate
	46	1000 mM Ammonium phosphate dibasic, 100 mM imidazole/Hydrochloric acid pH 8.0, 200 mM Sodium chloride
	48	1000 mM Potassium sodium tartrate, 100 mM MES/Sodium hydroxide pH 6.0

TABLE 2.2. Optimized Wizard 2 condition 33.

Original condition: 0.1 M Sodium citrate pH 5.5, 1 M Ammonium phosphate dibasic, 0.2 M Sodium chloride

pH	Condition contents		
5.0	0.1 M Sodium citrate	0.2 M Sodium chloride	0.5 M Ammonium phosphate
			0.8 M Ammonium phosphate
			1.2 M Ammonium phosphate
			1.4 M Ammonium phosphate
			1.6 M Ammonium phosphate
5.5	0.1 M Sodium citrate	0.2 M Sodium chloride	0.5 M Ammonium phosphate
			0.8 M Ammonium phosphate
			1.2 M Ammonium phosphate
			1.4 M Ammonium phosphate
			1.6 M Ammonium phosphate
6.0	0.1 M Sodium citrate	0.2 M Sodium chloride	0.5 M Ammonium phosphate
			0.8 M Ammonium phosphate
			1.2 M Ammonium phosphate
			1.4 M Ammonium phosphate
			1.6 M Ammonium phosphate
5.0	0.1 M Sodium citrate	0.2 M Sodium chloride	1.0 M Ammonium phosphate
6.0			
5.5	0.1 M Sodium citrate	0.1 M Sodium chloride	1.0 M Ammonium phosphate
		0.150 M Sodium chloride	
		0.250 M Sodium chloride	
		0.300 M Sodium chloride	

Table 2.3. Optimized Wizard 2 condition 37

Original condition: 0.1 M Tris pH 7.0, 1 M Potassium sodium tartrate, 0.2 M Lithium sulfate

pH	Condition contents		
7.0	0.1 M Tris	0.5 M Potassium sodium tartrate	0.2 M Lithium sulfate
		0.8 M Potassium sodium tartrate	
		1.2 M Potassium sodium tartrate	
		1.4 M Potassium sodium tartrate	
		1.6 M Potassium sodium tartrate	
7.5	0.1 M Tris	0.5 M Potassium sodium tartrate	0.2 M Lithium sulfate
		0.8 M Potassium sodium tartrate	
		1.2 M Potassium sodium tartrate	
		1.4 M Potassium sodium tartrate	
		1.6 M Potassium sodium tartrate	
8.0	0.1 M Tris	0.5 M Potassium sodium tartrate	0.2 M Lithium sulfate
		0.8 M Potassium sodium tartrate	
		1.2 M Potassium sodium tartrate	
		1.4 M Potassium sodium tartrate	
		1.6 M Potassium sodium tartrate	
7.5	0.1 M Tris	1.0 M Potassium sodium tartrate	0.2 M Lithium sulfate
8.0			
7.0	0.1 M Tris	1.0 M Potassium sodium tartrate	0.1 M Lithium sulfate
			0.150 M Lithium sulfate
			0.250 M Lithium sulfate
			0.3 M Lithium sulfate

TABLE 2.4. Summary of VvDxr (native and metal-bound) data collection

The table summarizes native VvDxr and cut VvDxr structures in complex with Mn^{2+} data collection and processing. The numbers in parenthesis refer to the highest resolution shell.

PDB Accession code	5KQO	5KS1	5KRR
Diffraction source	APS (22BM)	APS (19ID)	APS (19ID)
Wavelength (Å)	1.000	0.979	0.979
Detector	Marmosaic 225 mm CCD	ADSC Q315r	ADSC Q315r
Space group	$C222_1$	$C222_1$	$C222_1$
a, b, c (Å)	65.5 148.9 244.1	64.1 149.3 243.8	64.8 149.1 242.5
Resolution range (Å)	50.0-2.35 (2.39-2.35)	50.0-2.40 (2.44-2.40)	50.0-2.50 (2.54-2.50)
σ Cutoff	-3 σ	-3 σ	-3 σ
Total No. of reflections	49916 (2482)	46042 (2108)	38225 (1840)
Completeness (%)	99.9 (100.0)	99.2 (92.4)	93.4 (91.3)
Redundancy	4.5 (4.6)	5.6 (5.0)	5.3 (5.4)
$I/\sigma(I)$	33.2 (4.7)	31.0 (2.7)	16.9 (2.9)
$R_{r.i.m.}$	0.067	0.068	0.088
$R_{p.i.m.}$	0.031	0.028	0.037
Overall *B* factor from Wilson plot ($Å^2$)	46.8	52.3	33.1
CC ½	0.948	0.934	0.917

Table 2.5: Summary of VvDxr in complex with Arginine and cut VvDxr

PDB Accession code	5KRV	5KRY
Diffraction source	22ID	22BM
Wavelength (Å)	1.000	1.000
Detector	Rayonix MX 300-HS	Marmosaic 225 mm CCD
Space group	$C222_1$	$C222_1$
a, b, c (Å)	49.8 93.0 128.4	49.5 92.1 128.6
Resolution range (Å)	50.0-2.30 (2.34-2.30)	50.0-2.30 (2.34-2.30)
σ Cutoff	-3 σ	-3 σ
Total No. of reflections	53084 (2578)	53399 (2621)
Completeness (%)	99.9 (99.8)	99.5 (98.2)
Redundancy	7. (7.5)	8.1 (7.4)
$I/\sigma(I)$	22.7 (1.6)	21(2.1)
$R_{r.i.m.}$	0.100	0.118
$R_{p.i.m.}$	0.038	0.037
Overall *B* factor from Wilson plot (Å^2)	51.3	49. 587
CC ½	0.859	0.859

Table 2.6: Summary of 5KQO, 5KRV, AND 5KRY refinement statistics

PDB Accession Code	5KQO	5KRV	5KRY
Resolution range (Å)	50-2.35 (37.23-2.35)	500-2.30 (28.34-2.30)	50.0-2.30 (35.84-2.30)
Completeness (%)	99.7 (99.50)	99.4 (99.5)	99.9 (99.9)
σ Cutoff		0	0
No. of reflections, working set	47370		50748
No. of reflections, test set	2455	2686	2571
Final R_{cryst}	0.232(0.185)		0.184 (0.186)
Final Rf_{free}	0.182 (0.210)		0.225 (0.216)
No. of non-H atoms	6209	6155	6343
Protein	5971	5913	5957
Ligand	35	67	16
Solvent	203	175	370
R.m.s. deviations			
Bonds (Å)	0.70	0.55	0.80
Angles (º)	0.82	0.74	0.85
Average B factors (Å^2)			
Protein	53	63	46
Ligand	55	65	55
Ramachandran plot			
Most favored (%)	98	99	99
Allowed (%)	2	1	1
Visible Residues			
Chain A	1-398	1-394	1-191, 193, 195-207, 209-348, 30-375, 377-400
Chain B	1-397	1-393	1-149, 151-195, 197-208, 210-229, 231-375, 377-397, 399-400

Table 2.7: Summary of 5KS1 AND 5KRR refinement statistics

PDB Code	5KS1	5KRR
Resolution range (Å)	50.0-2.40(29.8-2.39)	50.0-2.5 (37.58-2.50)
Completeness (%)	99.2 (98.9)	84.1 (84.1)
σ Cutoff	0	0
No. of reflections, working set	43578	1840
Final R_{cryst}	0.189	0.191 (0.192)
Final Rf_{ree}	0.191	0.227 (0.230)
No. of non-H atoms	6094	6150
Protein	5900	5918
Ligand	36	23
Solvent	158	209
R.m.s. deviations		
Bonds (Å)	0.97	0.80
Angles (º)	0.97	0.87
Average B factors (Å^2)		
Protein	82	39
Ligand	98	56
Ramachandran plot		
Most favored (%)	98	98
Allowed (%)	2	2
Visible Residues		
Chain A	1-118, 120-242, 245-327	1-195, 197/198, 202-346, 348, 350-351, 354-367, 367-374, 378-377-382, 384-397, 399-400, 402-405
Chain B	1-118, 120-25, 29-309, 311-327	1-195, 197-367, 369-375, 377-397, 399-400, 402-405

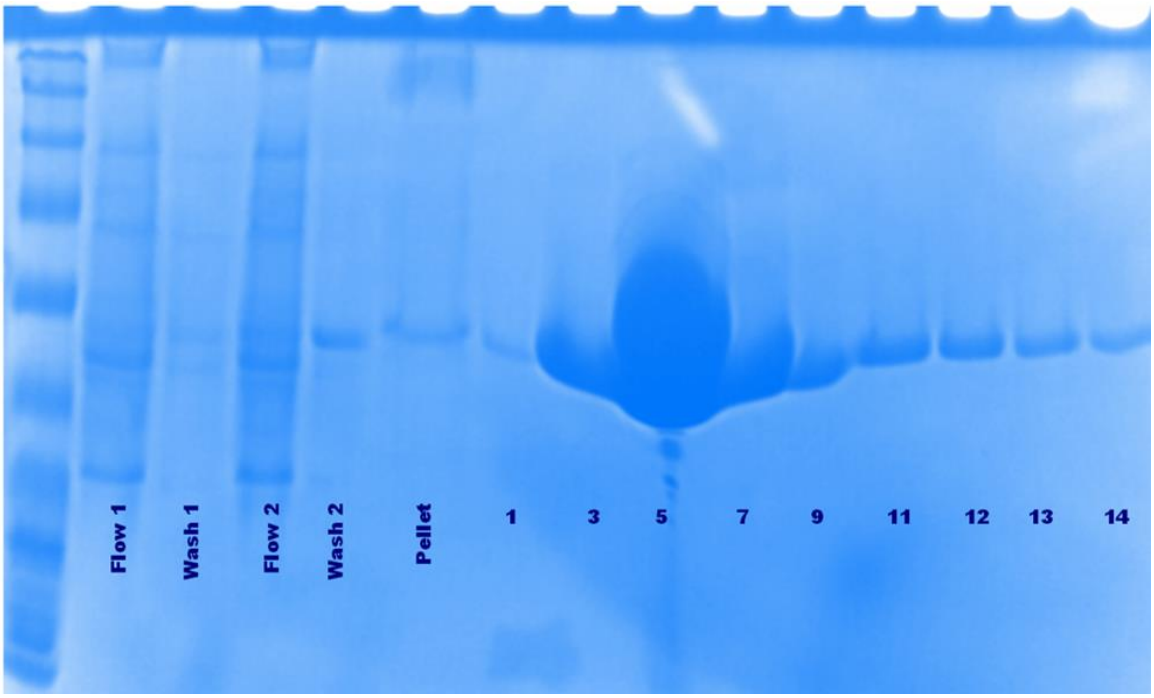

Figure 2.1: VvDxr gel electrophoresis. These results are typical of thepurification of VvDxr. The bands correspond to the expected molecular weight of the protein.

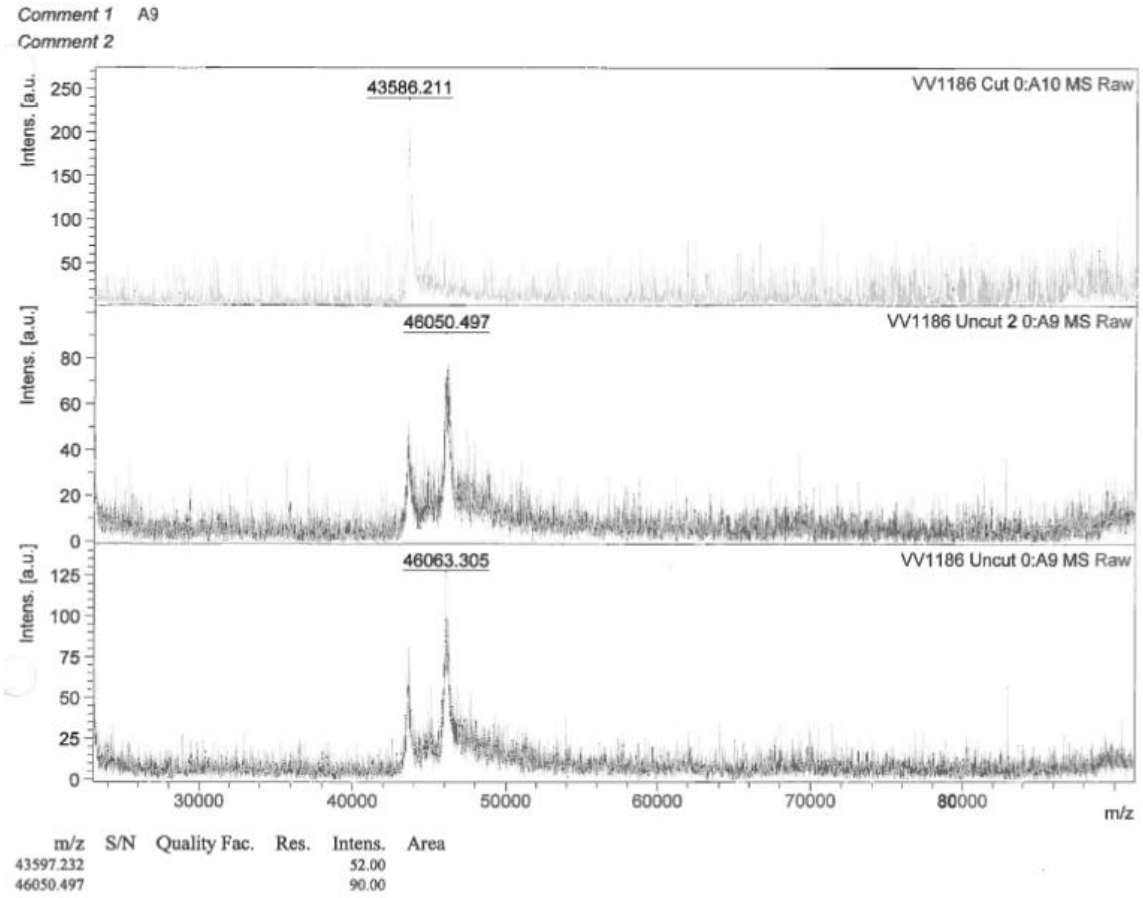

Figure 2.2. Mass spectrometry of uncut and cut VvDxr. The molecular weights shown correspond to the expected molecular weight of both the cut and uncut forms.

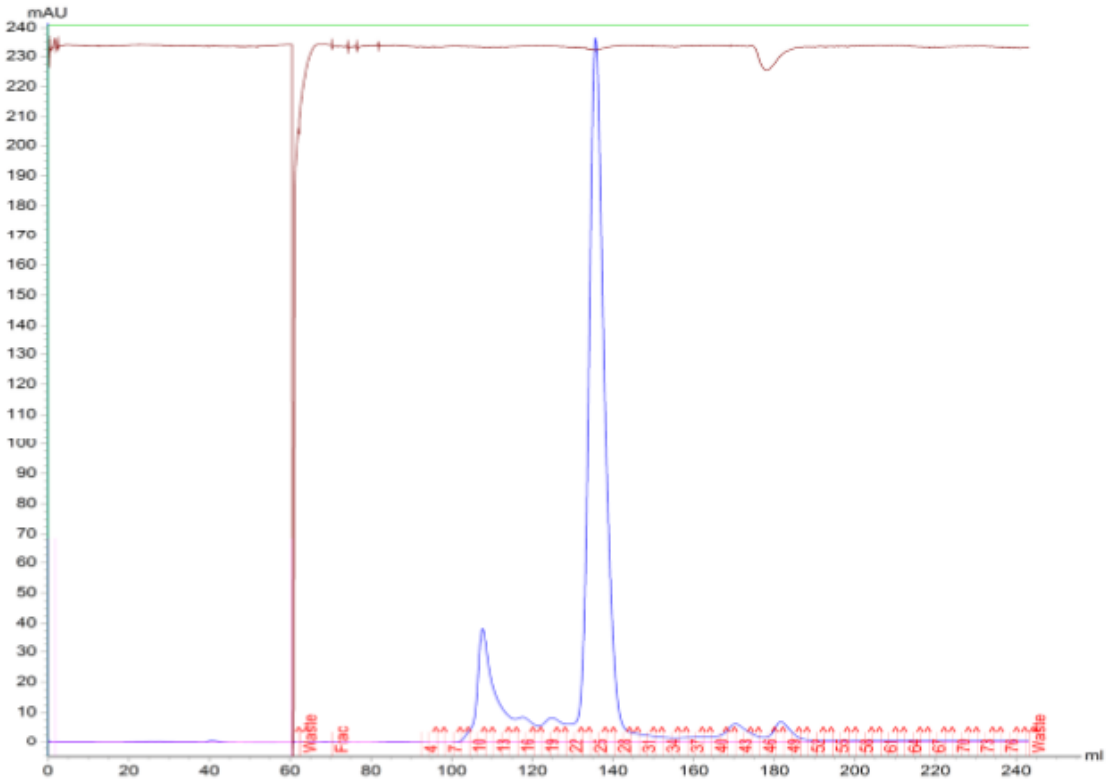

Figure 2.3 Chromatogram of cut VvDxr. The strong sharp peak reaching approximately 240 mAU also shows the protein is pure and present in abundant quantities. In comparing this elution profile to that of uncut VvDxr, there is a slight shift in where the protein elutes from the column.

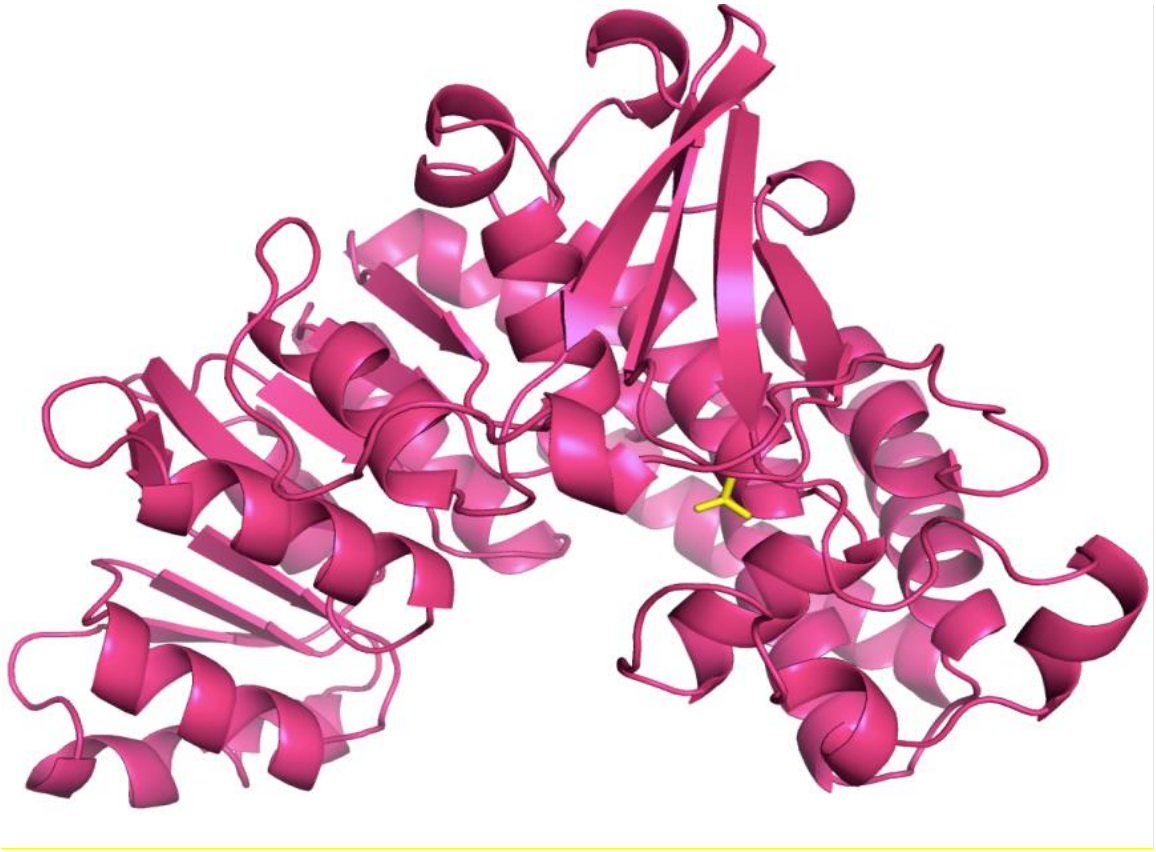

Figure 2.4. VvDxr monomer. The cartoon structure of VvDxr is depicted above. A phosphate ion is shown in the active site.

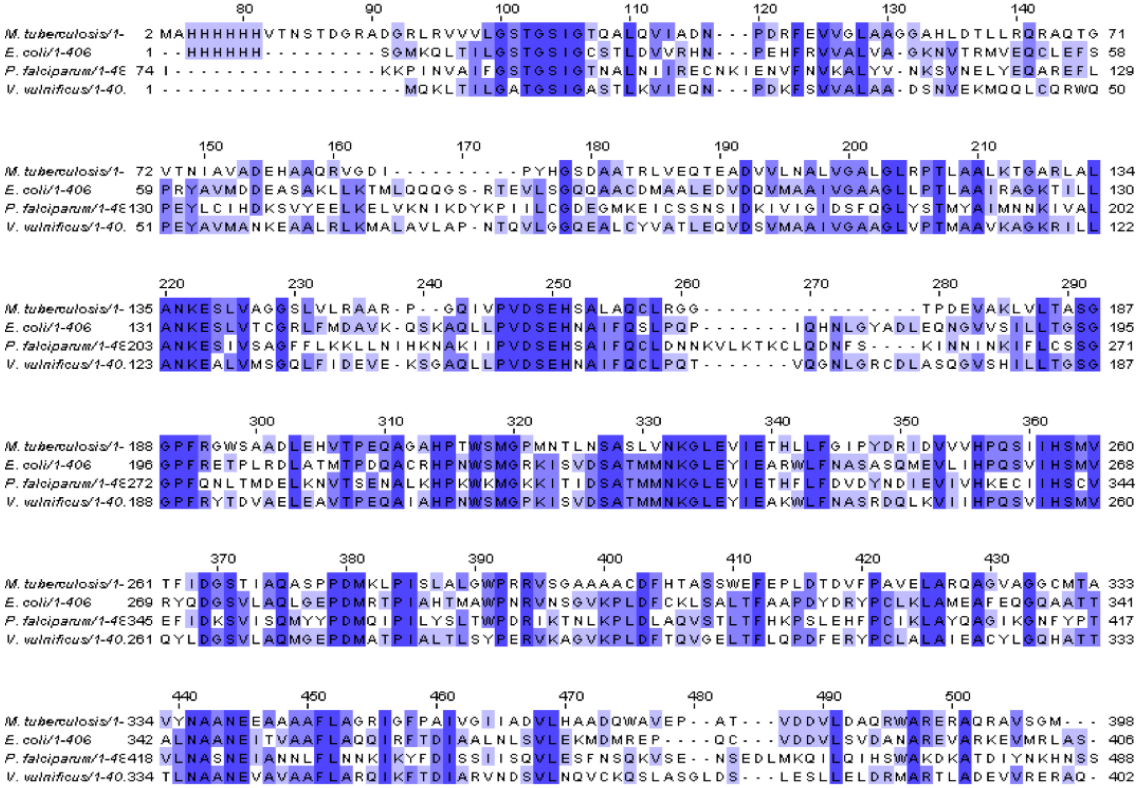

Figure 2.5. Multiple sequence alignment of Dxr homologs. This alignment was obtained from Kalign [20] to show Dxr enzymes from *M. tuberculosis, E. coli, P. falciparum, and V. vulnificus.* The percent identity when compared to *V. vulnificus* is 41% for *M. tuberculosis*, 62% for *E. coli,* and 37% for *P. falciparum.*

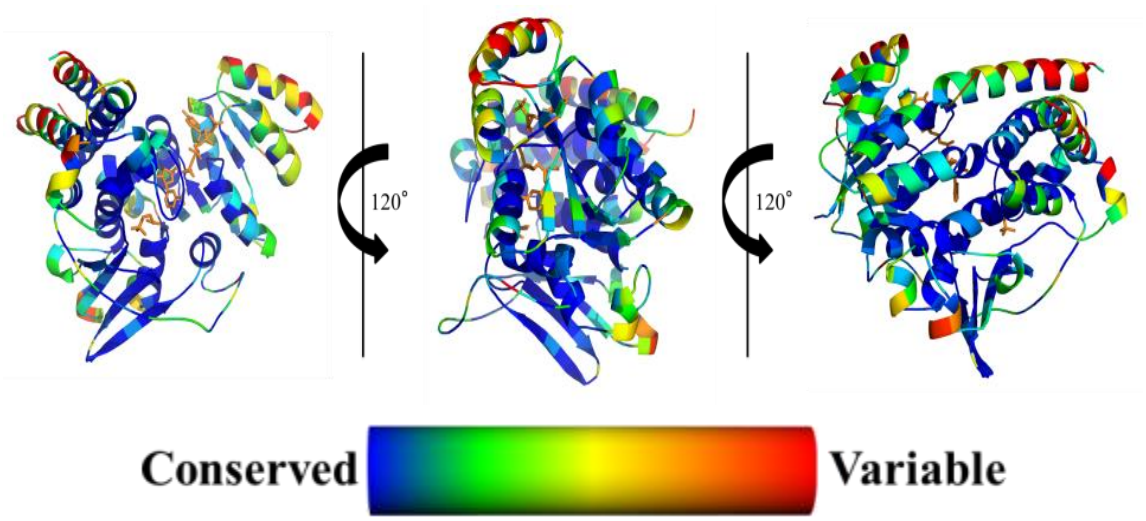

Figure 2.6: Conserved VvDxr residues. Above is a cartoon depiction showing the conserved residues of VvDxr mapped on protein structure [22-23]. *E. coli* Dxr (PDB ID: 2EGH) structure was used to show fosmidomycin and NADPH binding sites. Fosmidomycin and NADPH are shown as orange sticks. The highly conserved residues are located towards the active site and become more variable as it moves toward the surface of the enzyme [16].

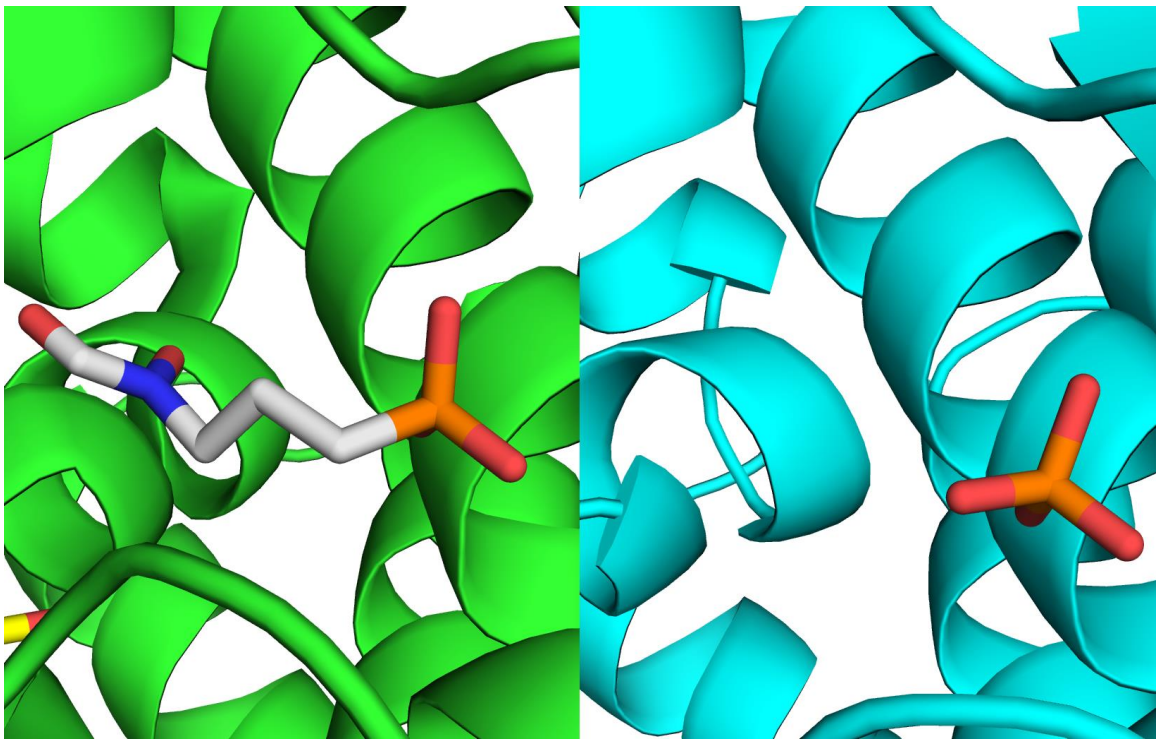

Figure 2.7 Juxtaposition of Dxr active sites. Left: PfDxr in complex with FR900098 (PDB code: 3AUA). Right: VvDxr with phosphate ion. The phosphate groups are in the same position in both structures.

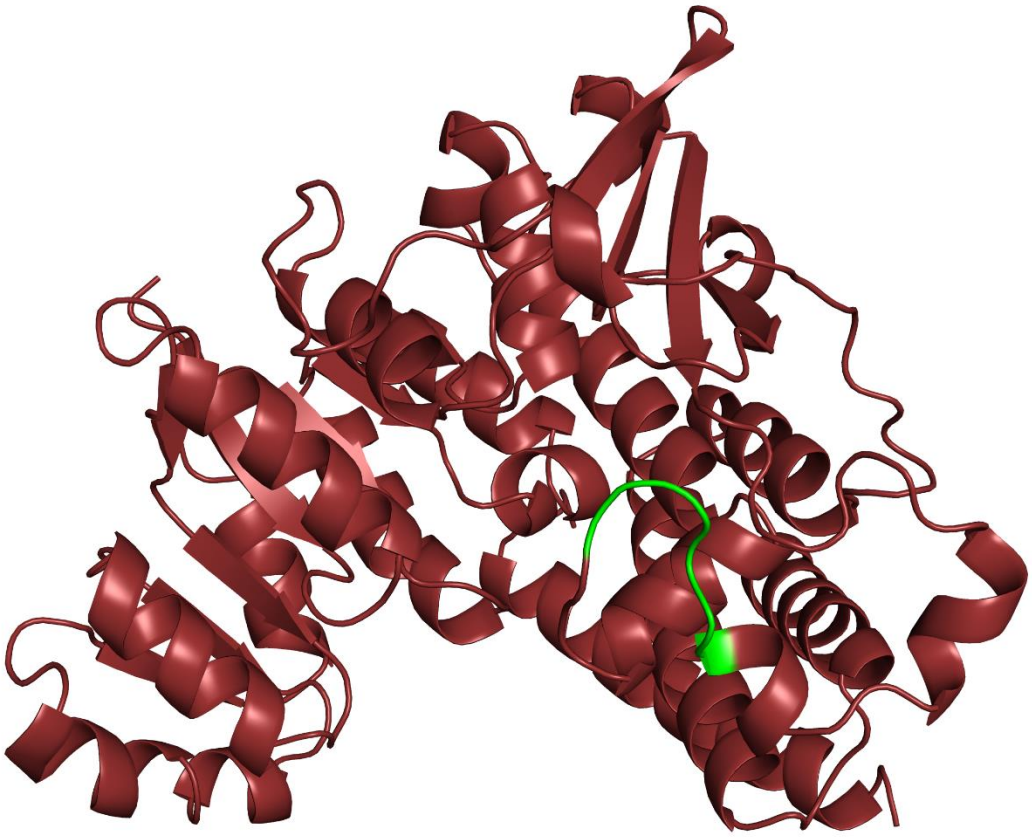

Figure 2.8. Flexible loop of VvDxr. The VvDxr monomer determined in our lab is shown with the flexible loop colored in green. The flexible loop moves over the active site upon ligand binding. Ussin *et al.*, in preparation

NaCl (M)															
	0	50	54	56	54	56	54	54	52	50	44	32	40		
	0.125	50	54	56	54	56	54	54	52	50	50	46	32	cut VvDxr	
	0.25	50	54	58	56	56	56	54	52	52	50	48	32		
	0.5	52	54	58	56	56	56	52	52	50	50	48	44		
	0.625	50	56	58	56	56	56	54	52	50	50	48	44		
	0.75	50	56	58	56	56	56	56	54	50	52	50	46		
	0.875	50	56	58	58	58	58	56	54	52	52	50	50		
	1	54	58	62	62	64	62	62	60	60	58	56	54		
NaCl (M)	0	48	52	54	52	52	50	50	48	32	40	30	30		
	0.125	48	52	54	52	52	52	50	48	44	32	32	30	uncut VvDxr	
	0.25	46	50	54	52	52	52	50	48	46	32	32	30		
	0.5	46	50	54	54	54	52	50	48	46	44	32	30		
	0.625	60	50	54	54	54	52	50	48	46	46	32	30		
	0.75	46	50	54	54	54	52	50	48	46	46	32	32		
	0.875	46	52	50	54	54	54	54	52	50	48	46	44		
	1	48	52	58	58	60	60	60	58	56	52	50	48		

Figure 2.9 Thermal stability: uncut vs cut VvDxr. The melting temperatures of the cut VvDxr are slightly higher indicating an increase in the thermal stability.

NaCl (M)	0	48	54	56	54	56	54	54	30	30	30	30	30	Vv1_uncut with 2
	0.125	48	52	56	54	56	54	30	30	30	30	30	30	mM Zinc (II) chloride
	0.25	46	52	56	54	56	56	54	30	30	30	30	30	
	0.5	30	50	56	54	56	56	54	30	30	30	30	30	
	0.625	30	30	56	56	56	56	54	30	30	30	30	30	
	0.75	44	50	56	56	58	56	54	30	30	30	30	30	
	0.875	46	30	56	56	58	58	56	30	30	30	30	30	
	1	30	30	58	58	60	60	60	58	58	30	30	30	
NaCl (M)	0	48	52	54	52	52	50	50	48	44	30	30	30	Vv1_uncut with 2
	0.125	48	50	52	52	52	52	50	48	44	32	32	30	mM Magnesium
	0.25	46	50	54	52	52	52	50	48	46	32	32	40	chloride
	0.5	46	50	54	54	52	52	50	48	46	32	32	40	
	0.625	46	50	54	54	54	52	52	48	46	46	32	40	
	0.75	46	50	54	54	54	54	52	50	48	46	32	32	
	0.875	46	50	54	54	54	52	54	50	50	48	46	44	
	1	46	52	58	58	50	58	60	58	54	52	48	52	
NaCl (M)	0	30	30	30	30	30	30	30	30	30	30	30	30	Vv1 uncut 2 mM
	0.125	30	30	30	30	30	30	30	30	30	30	30	30	Copper (II) chloride
	0.25	30	30	30	30	30	30	30	30	30	30	30	30	
	0.5	30	30	30	30	30	30	30	30	30	30	30	30	
	0.625	30	30	30	30	30	30	30	30	30	30	30	30	
	0.75	30	30	30	30	30	30	30	30	30	30	30	30	
	0.875	30	30	30	30	30	30	30	30	30	30	30	30	
	1	30	30	30	30	30	30	30	30	30	30	30	30	
NaCl (M)	0	48	52	54	52	50	50	50	48	46	32	32	30	Vv1_uncut with 2
	0.125	46	50	52	52	52	52	50	50	46	44	32	32	mM Calcium (II)
	0.25	46	50	54	52	52	52	52	50	48	32	32	32	chloride
	0.5	46	50	52	52	52	52	52	50	48	46	32	32	
	0.625	46	50	54	52	52	52	52	50	50	48	44	32	
	0.75	46	50	54	54	54	52	52	50	50	48	44	32	
	0.875	44	50	54	54	54	52	54	52	52	50	48	46	
	1	48	52	58	58	52	58	60	58	58	54	50	50	
NaCl (M)	0	48	52	54	52	54	56	58	58	56	50	30	32	uncut VvDxr 2 mM
	0.125	48	52	54	54	56	58	56	58	56	56	52	48	Manganese (II)
	0.25	46	50	54	54	56	58	58	58	58	56	90	90	chloride
	0.5	46	50	54	54	56	58	58	58	58	56	90	90	
	0.625	46	50	54	54	58	58	60	60	58	56	90	90	
	0.75	46	52	54	54	58	60	58	60	58	58	90	90	
	0.875	46	50	56	56	60	60	62	62	60	58	90	90	
	1	46	52	58	60	64	66	66	66	64	60	90	90	

Figure 2.10 Thermal stability: uncut VvDxr in presence of metals. The melting temperature of VvDxr increased in the presence of divalent cations, in particular manganese (II) chloride and magnesium (II) chloride. Copper (II) chloride caused VvDxr stability to immediately decrease. The 90° temperatures are due to experimental errors.

NaCl (M)	0	50	54	56	56	56	52	50	48	46	50	48	52		
	0.125	48	52	56	56	54	52	50	48	46	50	48	46	uncut VvDxr 2mM	
	0.25	46	52	54	54	54	52	50	48	46	50	48	46	NADPH 2mM Mn2+	
	0.5	46	52	54	54	54	52	50	48	48	52	48	48		
	0.625	44	50	54	54	54	52	50	48	48	50	50	48		
	0.75	44	50	54	54	54	52	50	50	48	50	50	48		
	0.875	44	50	54	56	54	54	52	50	50	52	50	50		
	1	44	52	56	58	58	58	56	56	54	54	54	54		
NaCl (M)	0	50	54	56	56	60	62	56	62	62	62	62	62		
	0.125	48	52	56	56	58	60	60	62	60	60	60	60	uncut VvDxr 2mM	
	0.25	46	52	54	56	58	60	60	54	60	60	60	60	NADPH 2mM Mg2+	
	0.5	46	52	54	56	58	60	60	60	60	60	60	60		
	0.625	46	52	54	58	58	60	62	62	60	60	60	60		
	0.75	46	50	54	56	58	60	62	62	62	62	60	62		
	0.875	44	50	56	58	60	62	62	62	62	62	62	60		
	1	44	52	56	62	62	64	64	64	62	62	62	64		

Figure 2.11 Thermal stability: uncut VvDxr in presence of NADPH and metals. VvDxr yielded higher melting temperatures when in the presence of both NADPH cofactor and either manganese (II) chloride or magnesium (II) chloride.

30	30	30	54	48	30	30	30	52	48	30	30		
30	30	30	30	30	30	42	46	30	30	30	48	uncut VvDxr DSF L2	
52	30	46	44	30	48	46	30	30	30	46	48		
46	30	30	56	30	46	48	30	30	30	30	30		
50	46	44	30	30	30	46	30	30	44	30	30		
48	46	30	30	44	48	30	30	30	54	30	46		
50	30	30	30	30	44	30	30	30	30	30	46		
30	30	48	50	46	50	48	48	30	48	30	48		
44	44	44	46	30	46	48	44	44	30	46	30		
30	30	30	30	44	44	30	46	44	44	58	30	uncut VvDxr DSF L3	
46	30	44	30	30	44	46	46	44	48	40	48		
46	50	32	46	46	46	50	46	56	44	30	62		
50	54	46	52	46	44	46	50	48	30	44	30		
30	30	46	30	48	52	46	44	44	50	62	46		
58	46	46	46	30	48	46	46	56	46	46	30		
52	30	56	46	44	46	48	46	44	48	60	48		
46	30	30	30	30	58	30	32	30	30	30	30		
44	46	30	30	50	30	30	30	30	46	30	30	uncut VvDxr DSF L4	
30	30	30	30	30	46	46	30	46	46	48	46		
46	30	30	48	30	46	30	30	30	30	46	30		
46	48	30	30	48	30	30	46	32	44	30	46		
30	30	30	48	46	30	30	40	30	44	30	30		
44	44	46	32	46	48	30	44	30	30	32	30		
30	30	48	40	48	48	30	30	44	44	30	44		

Figure 2.12 Thermal stability: VvDxr with ligand screens. VvDxr was tested with numerous ligands to identify small molecular compounds able to improve the protein's thermal stability.

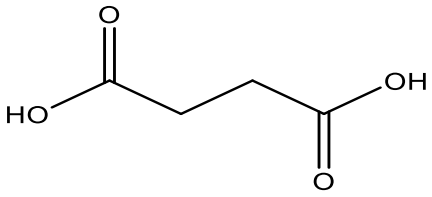

Succinate

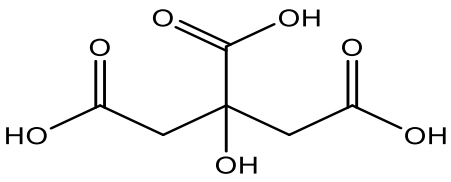

Citrate

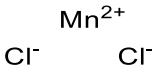

Manganese (II) chloride

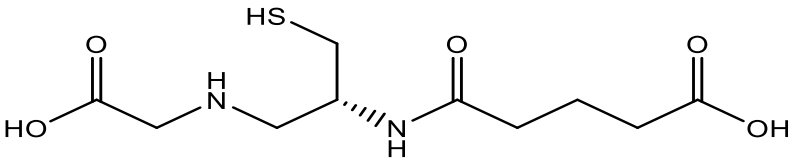

Reduced Glutathione

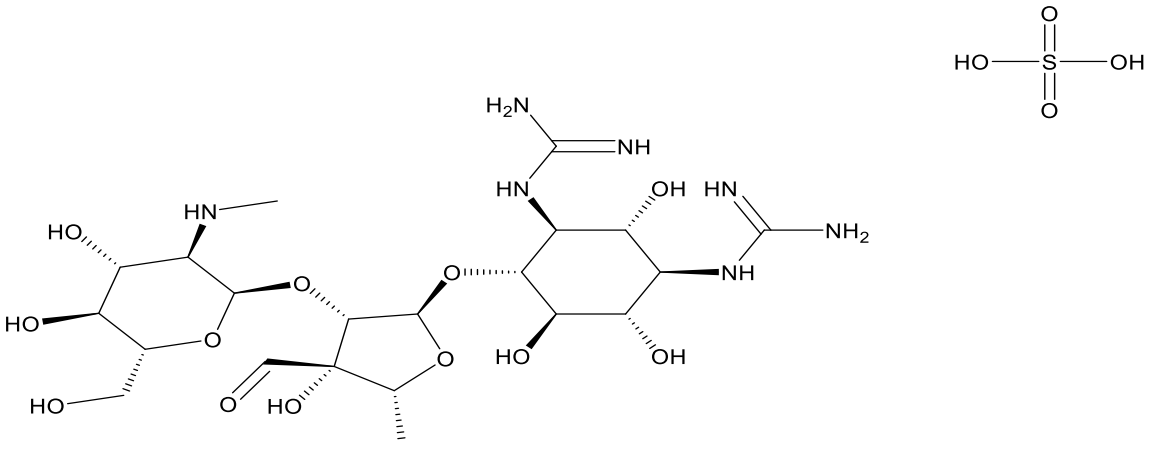

Streptomycin sulfate

Figure 2.13 Structure of ligands promoting thermal stability of VvDxr. These ligands were identified using DSF ligand screens

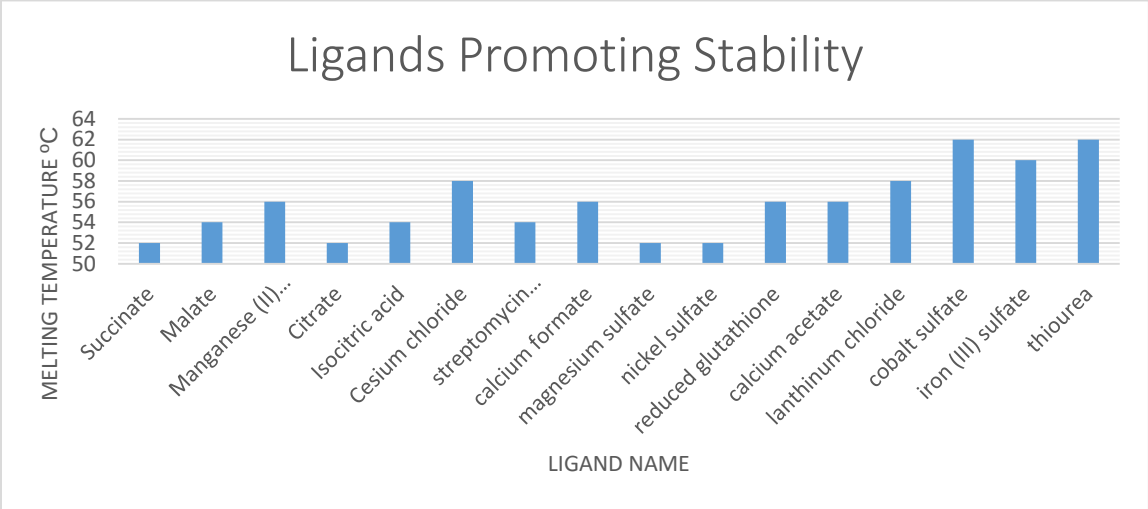

Figure 2.14. Graph of small molecules promoting thermal stability. This chart gives the melting temperature of VvDxr after being in the presence of the ligands named.

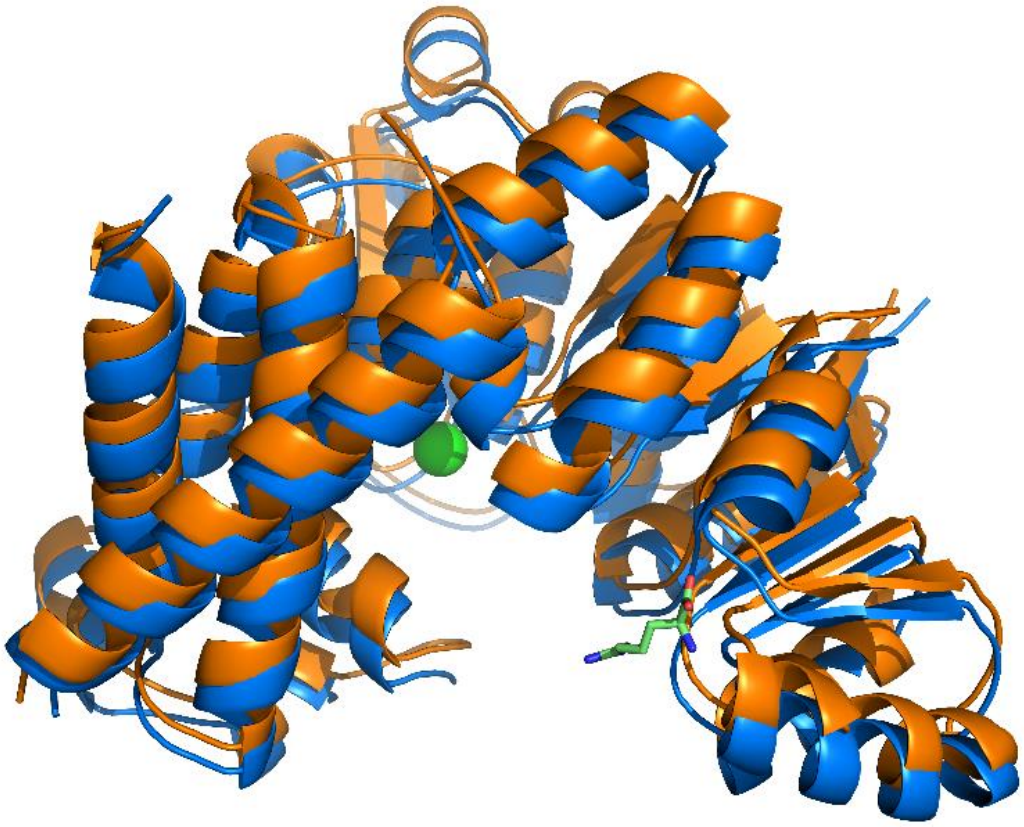

Figure 2.15. VvDxr in complex with Arginine. The blue structure is VvDxr in complex with arginine, and VvDxr in complex with Mn^{2i} is orange^{+}. Ligands are shown in green. By superposing the structures, manganese is located in the active site of the protein, while the arginine is not near the active site.

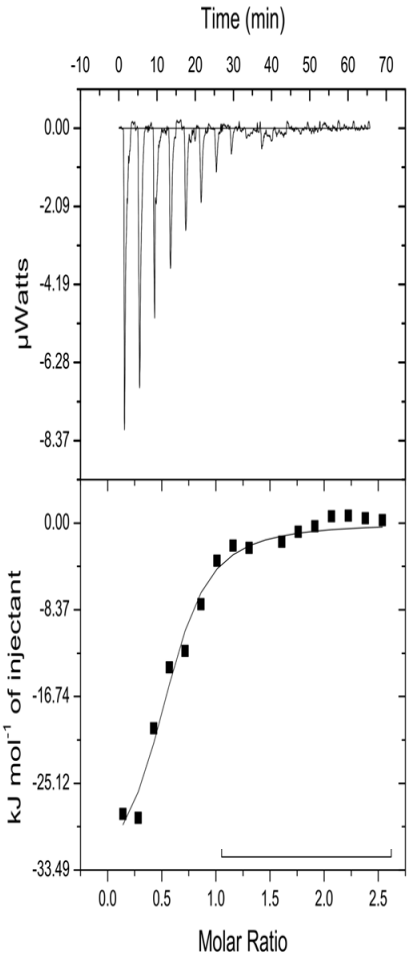

N (sites)	K (nM^{-1})	ΔH (kJ/mol)	ΔS (kJ/mol/ deg)	ΔG (kJ/mol)
0.54 ± 0.40	0.24 ± 0.01	-35 ± 3	-0.01	-31

Injector
1mM NADPH
Sample cell
0.05 mM VvDxr
10 mM Tris
50 mM NaCl
2 mM Mn^{2+}

Figure 2.16. ITC with NADPH and Manganese. The contents of the injector tell us how much ligand is used, and the contents of the sample cell give the concentration of the protein

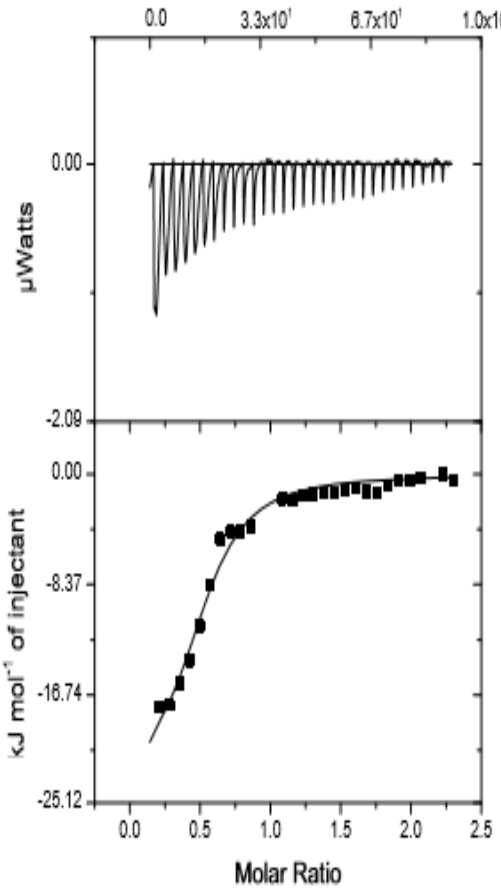

N (sites)	K (nM^{-1})	ΔH (kJ/mol)	ΔS (kJ/mol/deg)	ΔG (kJ/mol)
0.50 ± 0.03	3.25^{E-4}	-23.9 ± 1.6	.027	-32.1

Injector
1 mM 2,6 PDC
Sample
0.05 mM VvDxr
10 mM Tris
50 mM NaCl
2 mM Mg^{2+}

Figure 2.17. ITC with 2,6 PDC and Magnesium. The isotherm indicates there is protein-ligand binding.

Chapter 3
Materials and Methods

Bacterial Transformation

Recombinant VvDxr was ordered from DNA 2.0 (Mento Park, CA) in expression vector pJexpress411 with a cleavable, N-terminal polyhistidine tag (MHHHHHHSSGVDLGTENLYFQS↓GSG). This plasmid was transformed into *E. coli* strain BL21(DE3) and then grown overnight on Luria-Bertani (LB) agar plates supplemented with kanamycin. Colonies from the overnight growth were picked and grown. The GeneJet plasmid miniprep kit (Thermo Scientific, Wilmington, DE) was used to extract DNA from the culture. The concentration of the DNA was found using a NanoDrop UV/Vis (Thermo Scientific, Wilmington, DE) at an absorbance of 260 nm before being taken to the Engencore facility at the University of South Carolina for sequencing.

Overexpression and Purification of VvDxr

Cultures were grown to an OD_{600} of 0.8 then induced with 400 µM Isopropyl β-D-1-thiogalactopyranoside (IPTG) and grown overnight at 16°C. Culture media were centrifuged to pellet cells. Cells were re-suspended in 30 mL of lysis buffer (50 mM Tris, 500 mM NaCl, 10 mM imidazole, 2% glycerol, and 20 mM 2-mercaptoethanol) and lysed by sonication. The homogenate was centrifuged, and the half of the resulting supernatant was loaded onto Ni-NTA agarose (Thermo Scientific, Wilmington, DE) media equilibrated in wash buffer (50 mM Tris, 500 mM

NaCl, 30 mM imidazole, 2% glycerol, and 20 mM 2-mercaptoethanol). The column was washed with 10 column volumes of wash buffer before the remaining protein-containing supernatant was added to the column. The column was washed again with 10 column volumes of wash buffer. The protein was then eluted from the column using 'elution buffer' (50 mM Tris, 500 mM NaCl, 250 mM imidazole, 2% glycerol, and 20 mM 2-mercaptoethanol). Fractions were collected and protein-containing fractions were identified by SDS-PAGE. Those fractions containing protein were pooled and dialyzed in (10 mM Tris, pH 7.4, 150 mM NaCl, 5 mM 2-mercaptoethanol) overnight. Protein was concentrated using an Amicon Ultra concentrator (Millipore) with a 10, 000 Da molecular mass cutoff and purified on a Superdex 200 column attached to an ÄKTA Pure FPLC system (GE Healthcare). A solution composed of 10 mM Tris-HCl and 150 mM NaCl at pH 7.4 was used for gel filtration of VvDxr. After gel filtration, fractions containing protein were pooled and concentrated to about 9 mg/mL. Protein concentration was determined using the Bradford method [21]. His-tag cleavage was accomplished first by diluting uncut VvDxr to 1.5 mg/mL with dialysis buffer. TEV protease was added to the dilute protein-to-protease-to-protein ratio of 1:100 (w/w), then dialyzed overnight at 4°C. Following dialysis, VvDxr was purified again on the ÄKTA Pure FPLC system (GE Healthcare). After gel filtration, fractions containing protein were pooled and concentrated to 12 mg/mL.

VvDxr Crystallization

Crystallization of VvDxr was performed at 298 K. All initial crystallization experiments were performed using the hanging drop vapor diffusion methods

utilizing the Qiagen EasyXtal 15 well plates (Hilde, DE). The initial screening was performed on using Wizard Classic I and II screens (Rigaku, Bainbridge Island, WA). The well contained 400 µL of crystallization condition. The drops were formed by mixing 1 µL of protein solution and 1 µL of screen solution.

After obtaining initial crystals, VvDxr optimization experiments were performed using both the hanging and sitting drop vapor diffusion method. In the hanging drop diffusion method, 400 µL of the optimized crystallization screen was added to the well. The drops were once again formed by mixing 1 µL of protein solution and 1 µL of the optimized screen solution.

The initial sitting drop vapor diffusion experiments were performed utilizing NeXtal plates (Qiagen, Chatsworth, CA). 60 µL of the Index screen (Hampton Research, Aliso Viejo, CA) were added to the corresponding wells. The drops were formed by mixing 1 µL of protein solution and 1 µL of screen solution.

Differential Scanning Fluorimetry

Differential Scanning Fluorimetry (DSF) was used to determine the thermal stability of the. In this experiment, VvDxr is incubated with Sypro-Orange, a fluorescent dye which binds to the hydrophobic residues of the denaturing protein [22]. As the experiment proceeds, the protein is heated, exposing the hydrophobic residues. Thermal stability is determined based on the temperature at which they fluoresce.

Protein stability was determined through pH and salinity screening, and by using small molecular compounds. To determine protein stability using pH and

salinity, Sypro-Orange (Life Technologies, Grand Island, NY) was diluted 1:1000 in 1 mL of a 2 mg/mL VvDxr stock. The ninety-six buffer screen created in our lab contained conditions with pH increasing from 4.0 to 9.5 and increasing NaCl concentrations from 0.0 to 1.0 mM. The screen was transferred into their respective wells of the BioRad (Hercules, CA) Hardshell 96-well PCR plate along with VvDxr to make a 1:1 Sypro-Orange/VvDxr to buffer. The plate was then loaded into the BioRad (Hercules, CA) CFX96 real-time PCR machine and heated at 2°C increments per minute, starting at 30°C and ending at 90°C. As the VvDxr is heated, Sypro-Orange binds to the hydrophobic ends and fluoresces. The melting temperature of the protein is determined by the temperature at which the probe fluoresces. Dr. Nicholas Mank (unpublished) developed a protocol for interpreting protein melting using the derivative results calculated by the CFX96 software. VvDxr stability was also tested by the same method previously described using small molecular compounds. The compound screens were developed by solubilizing the compounds before putting them in Tris buffer at pH 7.5. The result is three hundred and eighty-four conditions divided into four separate screens. Appendix I gives a list of these conditions.

Isothermal Titration Calorimetry

Isothermal titration calorimetry was performed to determine if ligand to protein to protein binding was occurring and to study the thermodynamics of the binding. Ligands were dissolved in dialysis buffer containing 10 mM Tris, 50 mM NaCl, and either 5 mM Magnesium (II) chloride or Manganese (II) chloride. A VP-ITC MicroCalorimeter (GE Healthcare) was used at 25 °C VvDxr was present in

micromolar concentrations and was loaded into the sample cell. The ligand-buffer mixture was loaded into the injector. The ligand is slowing injected into the sample cell containing the protein. The enthalpy change was measure based on ligand binding. Separate runs were conducted in which the thermodynamics of binding of VvDxr individually to NADPH, NADP, and divalent cations were tested. Data was processed by ORIGIN software. An isotherm was generated after each run, and the number of binding sites can be extrapolated from the point of inflection which is the dissociation constant [23].

Data Collection and Processing

VvDxr crystals were cryo-protected with well solution and cryo-cooled in liquid nitrogen prior to the diffraction experiments prior to being shipped to the Advanced Photon Source in Argonne National Laboratory (ANL) in Lemont, IL. Initial data was collected on Sector 22 BM of the Southeast Regional Collaborative Access Team (SER-CAT). Data processing was performed using HKL-2000 [24] software. Details for the data-collection statistics are shown in Tables 2 and 3.

Structure Determination and Validation

VvDxr structures were determined using HKL-3000 [24], MOLREP [25] and selected programs from CCP4 suite [29]. Molecular replacement was used for phasing. The native structure of VvDxr was solved using the *Escherichia coli* Dxr homolog (PDB code: 1Q0L) as a starting model. Other structures of VvDxr were determined using Fourier synthesis. HKL-3000 and REFMAC [31] were used to refine all structures, followed by validation using COOT [32] and Molprobity [33].

All structures were deposited into the Protein Data Bank (PDB) and were given the following accession codes: 5KQO (native VvDxr); 5KS1 (His-tag cleaved VvDxr; soaked with fosmidomycin and Mn^{2+}); 5KRR (His-tag cleaved; soaked with Mn^{2+} and FR900098); 5KRY (His-tag cleaved with phosphate-free condition); and 5KRV (uncleaved; soaked with Arginine). Tables 4 and 5 provide a summary of the model refinement and validation.

References

1. Linkous, D. A., & Oliver, J. D. (1999). Pathogenesis of vibrio vulnificus. *FEMS Microbiology Letters*, *174*, 207-214. doi: 10.1111/j.1574-6968.1999.tb13570.x

2. Jones, M. K., & Oliver, J. D. (2009). Vibrio vulnificus: Disease and pathogenesis. *Infection and Immunity*,*77*(5), 1723-1733. doi: 10.1128/IAI.01046-08

3. FoodSafety.gov, (n.d.). *Vibrio infections*. Retrieved from U.S. Department of Health & Human Services website: http://www.foodsafety.gov/poisoning/causes/bacteriaviruses/vibrio_infections/

4. National Center for Emerging and Zoonotic Infectious Diseases (NCEZID), Division of Foodborne, Waterborne, and Environmental Diseases (DFWED). (2013). *Vibrio vulnificus*. Retrieved from Center for Disease Control and Prevention website: http://www.cdc.gov/vibrio/vibriov.html

5. Takahashi, S., Kuzuyama, T., Watanabe, H., & Seto, H. (1998). A 1-deoxy-d-xylulose 5-phosphate reductoisomerase catalyzing the formation of 2-c-methyl-d-erythritol 4-phosphate in an alternative nonmevalonate pathway for terpenoid biosynthesis.*Proceedings of the National Academy of Sciences of the United States of America*, *95*(17), 9879-9884. Retrieved from http://www.ncbi.nlm.nih.gov/pubmed/9707569

6. Kim, H., Kim, S., Jeong, H., Kim, T., Kim, J., Choy, H., Yi, K., & Rhee, J. (2011). Integrative genome-scale metabolic analysis of vibrio vulnificus for drug targeting and discovery. *Molecular Systems Biology*,*460*(7), 1-15. doi: 10.1038/msb.2010.115.

7. Heuston, S., Begley, M., Gahan, C., & Hill, C. (2012). Isoprenoid biosynthesis in bacterial pathogens.*Microbiology*, *2012*(158), 1389–1401. doi: 10.1099/mic.0.051599-0

8. Yajima, S., Hara, K., Sanders, J., Yin, F., Ohsawa, K., Wiesner, J., Jomaa, H., & Oldfield, E. (2004). Crystallographic structures of two bisphosphonate:1-deoxyxylulose-5-phosphate reductoisomerase

9. complexes. *Journal of the American Chemical Society*, *126*(35), 10824-10825. doi: 10.1021/ja040126m

10. Sweeney, A., Lange, R., Fernandes, R., Schulz, H., Dale, G., Douangamath, A., Proteau, P., & Oefner, C. (2005). The crystal structure of e.coli 1-deoxy-d-xylulose-5-phosphate reductoisomerase in a ternary complex with the antimalarial compound fosmidomycin and nadph reveals a tight-binding closed enzyme conformation. *Journal of Molecular Biology*, *345*(1), 115-127. doi: 10.1016/j.jmb.2004.10.030

11. Cheng, F., & Oldfield, E. (2004). Inhibition of isoprene biosynthesis pathway enzymes by phosphonates, bisphosphonates, and diphosphates. *Journal of Medicinal Chemistry* , *47*(21), 5149-5158. doi: 10.1021/jm040036s

12. Sem, D., Bertolaet, B., Baker, B., Chang, E., Costache, A., Coutts, S., Dong, Q., & Hansen, M. (2004). Systems-based design of bi-ligand inhibitors of oxidoreductases: Filling the chemical proteomic toolbox. *Chemistry and Biology*, *11*(2), 185-194. Retrieved from http://www.sciencedirect.com/science/article/pii/S1074552104000341

13. Leon, A., Liu, L., Hudock, M., Hall, P., Yin, F., Studer, D., Puam, K., & Morita, C. (2006). Isoprenoid biosynthesis as a drug target: bisphosphonate inhibition of escherichia coli k12 growth and synergistic effects of fosmidomycin. *Journal of Medicinal Chemistry* , *49*(25), 7331-7341. doi: 10.1021/jm060492b

14. Henriksson, L., Bjorkelid, C., Mowbray, S., & Unge, T. (2006). The 1.9 Å resolution structure of mycobacterium tuberculosis 1-deoxy-d-xylulose 5-phosphate reductoisomerase, a potential drug target.*ACS Medicinal Chemistry Letters*, *62*(7), 807-813. doi: 10.1107/S0907444906019196

15. Yajima, S., Nonaka, T., Kuzuyama, T., Seto, H., & Ohsawa, K. (2002). Crystal structure of 1-deoxy-d-xylulose 5-phosphate reductoisomerase complexed with cofactors: implications of a flexible loop movement upon substrate binding. *Journal of Biochemistry*, *131*(3), 313-317. Retrieved from http://www.ncbi.nlm.nih.gov/pubmed/11872159

16. Merckle, L., Andres-Gomez, A., Dick, B., Cox, R., & Godfrey, C. (2005). A fragment-based approach to understanding inhibition of 1-deoxy-d-xylulose-5-phosphate reductoisomerase. *Chembiochem*, *6*(10), 1866-1874. Retrieved from http://www.ncbi.nlm.nih.gov/pubmed/16116659

17. Humnabadkar V[1], Jha RK, Ghatnekar N, De Sousa SM. A high-throughput screening assay for simultaneous selection of inhibitors of

Mycobacterium tuberculosis 1-deoxy-D-xylulose-5-phosphate synthase (Dxs) or 1-deoxy-D-xylulose 5-phosphate reductoisomerase (Dxr). J Biomol Screen.;16(3):303-12. doi: 10.1177/1087057110394845.

18. Sweeney, A., Lange, R., Fernandes, R., Schulz, H., Dale, G., Douangamath, A., Proteau, P., & Oefner, C. (2005). The crystal structure of e.coli 1-deoxy-d-xylulose-5-phosphate reductoisomerase in a ternary complex with the antimalarial compound fosmidomycin and nadph reveals a tight-binding closed enzyme conformation. *Journal of Molecular Biology*, *345*(1), 115-127. doi: 10.1016/j.jmb.2004.10.030

19. Cheng, F., & Oldfield, E. (2004). Inhibition of isoprene biosynthesis pathway enzymes by phosphonates, bisphosphonates, and diphosphates. *Journal of Medicinal Chemistry* , *47*(21), 5149-5158. doi: 10.1021/jm040036s

20. Leon, A., Liu, L., Hudock, M., Hall, P., Yin, F., Studer, D., Puam, K., & Morita, C. (2006). Isoprenoid biosynthesis as a drug target: bisphosphonate inhibition of escherichia coli k12 growth and synergistic effects of fosmidomycin. *Journal of Medicinal Chemistry* , *49*(25), 7331-7341. doi: 10.1021/jm060492b

21. Yajima, S., Hara, K., Sanders, J., Yin, F., Ohsawa, K., Wiesner, J., Jomaa, H., & Oldfield, E. (2004). Crystallographic structures of two bisphosphonate:1-deoxyxylulose-5-phosphate reductoisomerase complexes. *Journal of the American Chemical Society*, *126*(35), 10824-10825. doi: 10.1021/ja040126m

22. Celniker G., Nimrod G., Ashkenazy H., Glaser F., Martz E., Mayrose I., Pupko T., and Ben-Tal N. 2013. ConSurf: Using Evolutionary Data to Raise Testable Hypotheses about Protein Function Isr. J. Chem. 2013 March 10, doi: 10.1002/ijch.201200096 PDF Online version

23. Goldenberg O., Erez E., Nimrod G., Ben-Tal N. 2009. The ConSurf-DB: Pre-calculated evolutionary conservation profiles of protein structures. Nucleic Acids Research, 2009, Vol. 37, Database issue D323-D327 PDF Online version

24. Lassmann, T., Fring, O., & Sonnhammer, E. (2009). Kalign2: high-performance multiple alignment of protein and nucleotide sequences allowing external features. *Europe Pubmed Central*, *37*(3), 858-865. doi: 10.1093/nar/gkn1006

25. Thermo Fisher Scientific Inc. Pierce Biotechnology. 2014. https://www.piercenet.com/instructions/2160129.pdf

26. Berggren, K. Steinber, T. Lauber, W. Carroll, J., Lopez, M., Chernokalskaya, E. , Zieske, L., Diwu, Z., Haugland, R., Patton, W., "A Luminescent Ruthenium Complex for Ultrasensitive Detection of Proteins Immobilized on Membrane Supports." *Analytical Biochemistry 276.2 (1999): 129-43, Web.*

27. Cai, G., Deng, L., Fryszczyn, B., Brown, N., Liu, Z., Jiang, H., Palzkill, T., & Song, Y. (2012). Thermodynamic investigation of inhibitor binding to 1-deoxy-d-xylulose-5-phosphate reductoisomerase. *ACS Medicinal Chemistry Letters*, *3*(6), 496-500. Retrieved from http://www.ncbi.nlm.nih.gov/pubmed/23050057

28. Z. Otwinowski and W. Minor, " Processing of X-ray Diffraction Data Collected in Oscillation Mode ", Methods in Enzymology, Volume 276: Macromolecular Crystallography, part A, p.307-326, 1997,C.W. Carter, Jr. & R. M. Sweet, Eds., Academic Press (New York).

29. Winn, M.D. *et al.*"Overview of the CCP4 suite acurrent developments:. doi: 10.1107/S0907444910045749. Acta Crys. D67. 235-242 (2011).International Union of Crystallography.

30. MOLREP: Vagin, A. A. & Teplyakov, A. (1997). J. Appl. Cryst. 30, 1022-1025. Vaguine, A. A., Richelle, J., Wodak, S. J. (1999). Acta Cryst. D55, 191-205.

31. REFMAC: Murshudov, G. N., Vagin, A. A. & D odson, E. J. (1997). Acta Cryst. D53, 240-255.

32. COOT: Emsley, P., Lohkamp, Bernhard, Scott, W., & Cowtan, K. (2010). Acta Cryst. 66, 486-501.

33. Chen et al. (2010) MolProbity: all-atom structure validation for macromolecular crystallography. Acta Crystallographica D66:12-21

34. Takenoya, M., Ohtaki, A., Noguchi, K., Endo, K., Sasaki, Y., Ohsawa, K., Yajima, S., & Yohda, M. (2010). Crystal structure of 1-deoxy-d-xylulose 5-phosphate reductoisomerase from the hyperthermophile thermotoga maritima for insights into the coordination of conformational changes and an inhibitor binding. *Journal of Structural Biology*,*170*(3), 532-539. doi: 10.1016/j.jsb.2010.03.015

35. Reuter, K., Sanderbrand, S., Jomaa, H., Wiesner, J., Steinbrecher, I., Beck, E., Hintz, M., & Klebe, G. (2001). Crystal structure of 1-deoxy-d-xylulose-5-phosphate reductoisomerase, a crucial enzyme in the non-mevalonate pathway of isoprenoid biosynthesis.*The Journal of Biological Chemistry*, *277*(7), 5378-5384. doi: 10.1074/jbc.M109500200

36. Li, H., Tian, J., Sun, W., Qin, W., & Gao, W. (2013). Mechanistic insights into 1-deoxy-d-xylulose 5-phosphate reductoisomerase, a key enzyme of the mep terpenoid biosynthetic pathway. *The FEBS Journal*, *280*(22), 5896-5905. doi: 10.1111/febs.12516.

Appendix A: DSF Ligand Screening Conditions

Table A.1. DSF ligand screen 2
(*All solutions also contain 0.05 M Tris (pH 7.5)*)

A1	0.1M Valine	D2	0.1M Sodium Cholate
A2	0.1M Alanine	D3	0.1M Sodium Pyrophosphate
A3	0.1M Arginine	D4	0.01M Manganese(II) Chloride
A4	0.1M Malate	D5	0.1M 2,6-Pyridine dicarboxylic acid ethyl ester
A5	0.1M Sodium Citrate	D6	0.1M Aspartate
A6	0.1M Threonine	D7	0.1M Adenine
A7	0.1M Glutamine	D8	0.1M Xylitol
A8	0.1M Isoleucine	D9	0.01M Cobalt(II) Chloride
A9	0.1M Succinate	D10	0.1M 2,6-Pyridine dicarboxylic acid
A10	0.1M Sodium Pyruvate	D11	0.1M Phenylalanine
A11	0.1M Glucose	D12	0.1M Uracil
A12	0.1M Lysine	E1	0.1M Mercaptosuccinate
B1	0.1M Asparagine	E2	0.1M γ-amino-butyric acid
B2	0.1M Homoserine	E3	0.1M 8-hydroxy-2-quinole carboxylic acid
B3	0.1M Cytosine	E4	0.1M Pimelic acid
B4	0.1M Glutamate	E5	0.1M Sodium Benzene 1,3-disulfonate
B5	0.1M Proline	E6	0.1M 6-oxo-pipecolinic acid
B6	0.1M Taurine	E7	0.1M Kanamycin
B7	0.1M Nicotinamide	E8	0.1M 5-amino-isophthalic acid
B8	0.1M Guanine	E9	0.1M Chelidanic acid
B9	0.1M Glycine	E10	0.1M 2-pyridine sulfonic acid
B10	0.1M Serine	E11	0.1M 2-proline
B11	0.1M Methionine	E12	0.1M Gly-gly
B12	0.1M 4-methylcatechol	F1	0.1M 3,3',5,5'-tetracarboxyl diphenalmethane
C1	0.1M Citrate	F2	0.1M 5-nitrofuroic acid
C2	0.1M Nicotinamide	F3	0.1M 4,5-dibromo-2-furoic acid
C3	0.01M Magnesium Chloride	F4	0.1M 5-sulfoisophthalic acid
C4	0.1M Leucine	F5	0.1M Betaine
C5	0.01M Zinc Chloride		
C6	0.01M Iron(III) Chloride		
C7	0.1M Sodium Pyrophosphate		
C8	0.1M Thymine		
C9	0.1M Sucrose		
C10	0.01M Calcium Chloride		
C11	0.1M Spermidine		
C12	0.1M 2,6-Pyridine dicarboxylic acid methyl ester		
D1	0.1M Tryptophan		

F6 0.1M isocitric acid lactone
F7 0.1M 3-aminobenzene sulfonic acid
F8 0.1M Chelidonic acid
F9 0.1M 1,3,5-benzene tricarboxylic acid
F10 0.1M isocitric acid
F11 0.1M p-coumaric acid
F12 0.1M 2,5-thiophene dicarboxylic acid
G1 0.1M Phosphoserine
G2 0.1M Tartaric acid
G3 0.1M Arabinose
G4 0.1M Chloramphenicol
G5 0.1M Naringin
G6 0.1M Caffeic acid
G7 0.1M 2,4-pyridine dicarboxylic acid
G8 0.1M 2,3-pyridine dicarboxylic acid
G9 0.1M 3,5-pyridine dicarboxylic acid
G10 0.1M 2,5-pyridine dicarboxylic acid
G11 0.1M Tyrosine
G12 0.1M Rutin
H1 0.1M Morin
H2 0.01M Copper(II) Chloride
H3 0.1M Maltose
H4 0.1M AMP
H5 0.1M Myo-inositol
H6 0.1M Ascorbic acid
H7 0.1M Thiamine
H8 0.1M Pimelic acid
H9 0.1M 3-aminobenzene sulfonic acid
H10 0.1M Melamine
H11 0.1M 2,5 FDC
H12 0.1M Cystine

Table A.2: DSF ligand screen 3
(*All solutions also contain 0.1 M Tris (pH 7.5)*)

A1	30% Methanol
A2	30% Ethanol
A3	30% DMSO
A4	40% Acetone
A5	30% Glycerol
A6	30% Ethylene Glycol
A7	0.1M Bromosuccinic acid
A8	0.1M Cytidine
A9	0.1M Cytidine in 100% Ethanol
A10	0.1M Sodium Deoxycholate
A11	0.1M Sodium Chloride
A12	0.1M Trimesic acid
B1	0.1M Histidine HCl
B2	0.1M 1,4-butanediol
B3	0.1M Neopentyl Alcohol
B4	0.1M Cadmium Chloride
B5	0.1M Malonic acid
B6	0.1M 3,4-dihydroxybenzoic acid
B7	0.1M CHES
B8	0.1M MOPS
B9	0.1M L-norvaline
B10	0.1M 1,6-hexanediol
B11	0.1M Lanthanum Chloride Heptahydrate
B12	0.1M Vanillin
C1	0.1M Kanamycin Sulfate
C2	0.1M N,N-dimethylglycine
C3	0.1M Salicylic acid
C4	0.1M 3-hydroxy-2-naphthoic acid
C5	0.1M Tris(hydroxymethyl)aminomethane
C6	0.1M CAPS
C7	0.1M Ethylene Glycol
C8	0.1M Chloroquine
C9	0.1M Potassium Thiocyanate
C10	0.1M Fast Garnet GBC Salt
C11	0.1M N,N-dimethyldecylamine-N-oxide
C12	0.1M 1,4-butanediphosphonic acid
D1	0.1M Lithium Acetate
D2	0.1M Magnesium Nitrate
D3	0.1M Fast Violet B Salt
D4	0.1M β-NAD
D5	0.1M α-lactose monohydrate
D6	0.1M Guanidine Thiocyanate
D7	0.1M Sodium Bisulfate
D8	0.1M BOC-L-serine
D9	0.1M Glutathione (reduced)
D10	0.1M PIPES
D11	0.1M Sodium Bicarbonate
D12	0.1M Thiourea
E1	0.1M α-naphthyl acid phosphate
E2	0.1M Streptomycin Sulfate
E3	0.1M Hexamine Cobalt(III) Chloride
E4	0.1M Magnesium Sulfate
E5	0.1M Lithium Sulfate
E6	0.1M 4-dimethylaminopyridine
E7	0.1M S-(-)-2-bromopropionic acid
E8	0.1M O-phospho-DL-serine
E9	0.1M Nickelous Acetate
E10	0.1M Tetraamine Copper(II) Sulfate
E11	0.1M Potassium Tetrachloroplatinate
E12	0.1M Ammonium Cerium(IV) Nitrate
F1	0.1M Chromium Acetate
F2	0.1M Trifluoroacetic acid Silver Salt
F3	0.1M Nicotinic acid
F4	0.1M Trimethyl Lead Acetate
F5	0.1M Propylenediphosphonic acid
F6	0.1M Nickel Sulfate
F7	0.1M Tetraethylpropylene-1,3-diphosphonic acid
F8	0.1M 1,6-hexane bis-phosphonic acid
F9	0.1M Cesium Fluoride
F10	0.1M Strontium Nitrate
F11	0.1M Cobaltous Sulfate

F12 0.1M Glutathione
G1 0.1M Cerous Chloride
G2 0.1M Sodium Molybdate(III) dehydrate
G3 0.1M Thallium(I) Nitrate
G4 0.1M Cesium Chloride
G5 0.1M Iodoacetamide
G6 0.1M Phosphonoacetic acid
G7 0.1M 2,6-naphthalenedisulfonic acid disodium salt
G8 0.1M Propionic acid
G9 0.1M Calcium Acetate
G10 0.1M 1,1,3,3-tetramethylurea
G11 0.1M Adonitol
G12 0.1M Nicotinamide
H1 0.1M GMP
H2 0.1M Cacodylic acid
H3 0.1M Calcium Formate
H4 0.1M Lithium Citrate
H5 0.1M Imidazole
H6 0.1M Lithium Chloride
H7 30% Dextrose
H8 0.1M Sodium Sulfate
H9 0.1M Thymidine
H10 0.1M Potassium Hydrogen Phthalate
H11 0.1M Ferrous Sulfate
H12 0.1M Hydroxylaminohydrochloride

Table A.3: DSF ligand screen 4
(*All solutions also contain 0.1 M Tris (pH 7.5)*)

A1	0.1M ADA (N-2-acetamide-2-iminodiacetic acid)
A2	0.1M trans-4,5-dihydroxy-1,2-dithiane
A3	0.1M 1-naphthalene acetic acid
A4	0.1M β-alanine
A5	0.1M Potassium Chloride
A6	0.1M Cerium(III) Chloride Heptahydrate
A7	0.1M Lithium Fluoride
A8	0.1M 5,5'-dithiobis(2-nitrobenzoic acid)
A9	0.1M 1,2,4,5-benzenetetracarboxylic acid
A10	0.1M Cyclohexylsuccinic acid
A11	0.1M 6-(methoxycarbonyl) picolinic acid
A12	0.1M CHAPS
B1	0.1M trans-cinnamic acid
B2	0.1M Sulfonic acid
B3	0.1M Sodium 3-sulfobenzoate
B4	0.1M 8-anilino-1-naphthalene sulfonic acid
B5	0.1M N-bromosuccinimide
B6	0.1M Terephthalic acid
B7	0.1M Chlorosuccinic acid
B8	0.1M Guanidine HCl
B9	2% Triton-X114
B10	0.1M L-serine
B11	0.1M Dextrose Anhydrous
B12	0.1M Sodium Tartrate Dihydrate
C1	0.1M Sodium Acetate Trihydrate
C2	0.1M PEG 400
C3	10% Poly(vinyl Alcohol)
C4	0.1M 1,2-dihydroxybenzene
C5	0.1M Sodium Malonate Dibasic Monohydrate
C6	0.1M 5-aminovaleric acid
C7	0.05M PEG 8000
C8	0.1M PEG 200
C9	0.1M NDSB-221
C10	0.1M NDSB-201
C11	0.1M 2,2-dimethylsuccinic acid
C12	0.05M PEG 6000
D1	0.1M PEG 4000
D2	0.1M NDSB-256
D3	0.1M Glycerol
D4	0.1M MES Free Acid Monohydrate
D5	0.1M PEG 2000 MME
D6	0.1M PEG 5000 MME
D7	0.1M NDSB-195
D8	0.1M Phthalic acid
D9	0.1M 2-methyl-2,4-pentanediol
D10	0.1M PEG 3350
D11	0.1M PEG 1000
D12	0.1M 2-hydroxy-2-(2-isopropoxy-2-oxoethyl) succinic acid
E1	0.1M 6-(ethoxylcarbonyl) Picolinic acid
E2	0.1M EDTA
E3	0.1M Potassium Sulfate
E4	0.1M Sodium Carbonate
E5	0.06M N-bromosuccinic acid in 40% Acetone
E6	0.07M Thymol in 30% Ethanol
E7	0.07M 2-adamantanone in 30% Methanol
E8	0.07M N-bromosuccinic acid in 30% DMSO
E9	0.01M 2,2'-azino-bis(3-ethylbenzothiazoline-6-sulfonic acid)
E10	0.07M Sodium Tetraborate in 30% Ethylene Glycol
E11	0.1M Mellitic acid
E12	0.1M methyl-6-hydroxymethyl-2-carboxylate pyridine
F1	0.07M Decanoic acid in 30% Ethanol
F2	0.01M Tetrasodium Pyrophosphate

F3 0.07M Thymine in 30% Methanol
F4 0.01M Calcium Gluconate
F5 0.01M D-2-phosphoglyceric acid
F6 0.07M Hexadecyltrimethylammonium bromide in 30% Ethanol
F7 0.07M 1,3-dicyclohexyl-carbodiimide in 30% Ethanol
F8 0.01M Asparagine
F9 0.01M Calcium Sulfate
F10 0.07M 2,4-dibromophenol in 30% Ethanol
F11 0.01M Adenine
F12 0.07M 3-amino-4-hydroxybenzoic acid in 30% Ethanol
G1 0.06M 3-amino-4-hydroxybenzoic acid in 40% Acetone
G2 0.01M Phenylurea
G3 0.06M Chloramphenicol in 40% Acetone
G4 0.07M Thymine in 30% DMSO
G5 0.06M 3-indoleacetic acid in 40% Acetone
G6 0.07M Melamine in 30% Glycerol
G7 0.07M 5-iodosalicylic acid in 30% Ethanol
G8 0.07M 4-aminobiphenyl in 30% DMSO
G9 0.01M Magnesium Citrate
G10 0.07M Caffeine in 30% Ethanol
G11 0.07M Quinine HCl in 30% Ethanol
G12 0.07M Rhodanine in 30% Ethanol
H1 0.1M (2R,6S)-2,6-piperdinedicarboxylate
H2 0.1M 8-aminooctanoic acid
H3 0.1M O-phospho-L-serine
H4 0.1M Diphenylamino-4-sulfonic acid
H5 0.1M Phytic acid
H6 0.1M TCEP HCl
H7 0.01M Samarium Sulfate
H8 0.01M Dibutylthiourea
H9 0.07M 2,6-dibromophenol in 30% Ethanol
H10 0.07M Kinetin in 30% DMSO
H11 0.07M 1-phenyl-2-thiourea in 30% Ethanol
H12 0.01M Thallium Chloride

Appendix B: Optimized Index Conditions

Table B.1: Optimized Index condition

Index C10: 1.0 M Succinic Acid pH 7.0, 0.1 M HEPES pH 7.0, 1 % w/v PEG 2000						
0.5 M Succinic acid, 1 % PEG 2000	0.8 M Succinic acid, 1 % PEG 2000	0.9 M Succinic acid, 1 % PEG 2000	1.0 M Succinic acid, 1 % PEG 2000	1.1 M Succinic acid, 1 % PEG 2000	1.2 M Succinic acid, 1 % PEG 2000	PH = 7, HEPES = 0.1 M, different PEG and Succinic acid concentrations
0.5 M Succinic acid, 2 % PEG 2000	0.8 M Succinic acid, 2 % PEG 2000	0.9 M Succinic acid, 2 % PEG 2000	1.0 M Succinic acid, 2 % PEG 2000	1.1 M Succinic acid, 2 % PEG 2000	1.2 M Succinic acid, 2 % PEG 2000	
0.5 M Succinic acid, 4 % PEG 2000	0.8 M Succinic acid, 4 % PEG 2000	0.9 M Succinic acid, 4 % PEG 2000	1.0 M Succinic acid, 4 % PEG 2000	1.1 M Succinic acid, 4 % PEG 2000	1.2 M Succinic acid,	
0.5 M Succinic acid, 3% PEG 2000	0.8 M Succinic acid, 3% PEG 2000	0.9 M Succinic acid, 3 % PEG 2000	1.0 M Succinic acid, 3 % PEG 2000	1.1 M Succinic acid, 3 % PEG 2000	1.2 M Succinic acid,	
PH 7.6, PEG 1 %	PH 7.6, PEG 2%	PH 7.6 PEG 3%	PH 7.6 PEG 4%	PH 7.6 PEG 5%		Same Succinic acid concentration= 1 M, HEPES = 0.1 M, different PEG concentration and pH
PH 7.2 PEG 1 %	PH 7.2 PEG 2%	PH 7.2 PEG 3%	PH 7.2 PEG 4%	PH 7.2 PEG 5%		
PH 6.8 PEG 1 %	PH 6.8 PEG 2%	PH 6.8 PEG 3%	PH 6.8 PEG 4%	PH 6.8 PEG 5%		
PH 6.4 PEG 1 %	PH 6.4 PEG 2%	PH 6.4 PEG 3%	PH 6.4 PEG 4%	PH 6.4 PEG 5%		